PLASTID STATUS INFLUENCES CELL FATE DECISIONS AT THE PLANT SHOOT APEX

Margaret E. Wilson[1], R. Howard Berg[2] and Elizabeth S. Haswell[1]*

[1]Department of Biology, Mailbox 1137, Washington University in Saint Louis, Saint Louis, MO, USA

[2]Donald Danforth Plant Science Center, 975 North Warson Rd., Saint Louis, MO, USA

*Corresponding author

SUMMARY STATEMENT

Plastid osmotic stress influences cell fate decisions at the plant shoot apex via two established mechanisms that control proliferation: the cytokinin/WUSCHEL stem cell identity loop and a plastid-to-nucleus signaling pathway.

ABSTRACT

The balance between proliferation and differentiation in the plant shoot apical meristem is controlled by regulatory loops involving the phytohormone cytokinin and stem cell identity genes. Concurrently, cellular differentiation in the developing shoot is coordinated with the environmental and developmental status of plastids within those cells. Here we employ an *Arabidopsis thaliana* mutant exhibiting constitutive plastid osmotic stress to investigate the molecular and genetic pathways connecting plastid status with cell fate decisions at the shoot apex. *msl2 msl3* mutants exhibit dramatically enlarged and deformed plastids in the shoot apical meristem, and develop a mass of callus tissue at the shoot apex. Callus production in this mutant is characterized by increased cytokinin levels, the down-regulation of cytokinin signaling inhibitors *ARR7* and ARR15, and induction of the stem cell identity gene *WUSCHEL* and is reduced in the absence of the cytokinin receptor AHK2. Furthermore, plastid stress-induced apical callus requires elevated plastidic ROS, ABA biosynthesis, and retrograde signaling proteins GUN1 and ABI4. These results establish a functional link between the cytokinin/WUS pathway and retrograde signaling in controlling cell fate at the shoot apex.

32

33 **INTRODUCTION**

34

35 How cell fate is determined is a fundamental question. The development of land plants provides a
36 unique opportunity to study this decision-making process, as plant cell identity is highly plastic
37 (Gaillochet and Lohmann, 2015). A classic illustration of plant cell pluripotency is the ability to produce
38 a mass of undifferentiated cells referred to as callus. Callus results from the reacquisition of an
39 undifferentiated state or the initial inability to differentiate properly, and is generated by a variety of
40 mechanisms which include wounding and exposure to pathogens (Ikeuchi et al., 2013). The best-
41 understood and most widely employed way to induce the production of callus is treatment with two
42 phytohormones, cytokinin (CK) and auxin (Skoog and Miller, 1957).

43

44 In addition, land plants maintain the ability to develop new organs continuously during their lifespan.
45 This is made possible by small self-renewing pools of undifferentiated cells, called meristems, from
46 which new organs are derived as the plant grows (Aichinger et al., 2012; Gaillochet and Lohmann,
47 2015). Above ground, the maintenance and regulation of the shoot apical meristem (SAM) is critical
48 for the proper specification and positioning of leaves (Barton, 2010). SAM identity requires both the
49 imposition of stem cell fate by the WUSCHEL(WUS)/CLAVATA(CLV) signaling circuit (Schoof et al.,
50 2000) (Fletcher et al., 1999) and the suppression of differentiation by SHOOTMERISTEMLESS (STM)
51 (Endrizzi et al., 1996; Long et al., 1996).

52

53 CK plays a key role in the function of the SAM. In the central zone (CZ), CK promotes proliferation,
54 while auxin promotes differentiation in the peripheral zone (PZ) (Schaller et al., 2015). Localized CK
55 perception and response specifies the organizing center of the SAM, also the region of *WUS*
56 expression (Chickarmane et al., 2012; Gordon et al., 2009; Zurcher et al., 2013). WUS activity
57 maintains itself through a positive feedback loop involving CK response via Type-A Arabidopsis
58 Response Regulators (ARRs), key negative regulators of CK signaling (Leibfried et al., 2005; Schuster
59 et al., 2014; To et al., 2007; Zhao et al., 2010). In addition, auxin serves to promote CK signaling in the
60 meristem by repressing ARRs (Zhao et al., 2010). Thus, auxin and CK levels interact with the
61 WUS/CLV pathway to regulate the balance between cell differentiation and cell proliferation both in
62 callus and in the SAM (Gaillochet and Lohmann, 2015; Ikeuchi et al., 2013).

63

64 Shoot development also depends on plastids, endosymbiotic organelles responsible for
65 photosynthesis, amino acid, starch, and fatty acid biosynthesis and the production of many hormones

66 and secondary metabolites (Neuhaus and Emes, 2000). Plastids are present in almost every plant cell,
67 and develop specialized characteristics associated with the cell type in which they reside (Jarvis and
68 Lopez-Juez, 2013). As cells leave the SAM and take on the appropriate cell identity within leaf
69 primorida, the small, undifferentiated plastids, called proplastids, inside them must also differentiate,
70 usually into chloroplasts.
71
72 Many mutants lacking functional plastid-localized proteins exhibit secondary defects in leaf cell
73 specification ((Larkin, 2014; Luesse et al., 2015; Moschopoulos et al., 2012), providing genetic
74 evidence that normal leaf development depends upon plastid homeostasis. The integration of plastid
75 differentiation into the process of development likely requires tightly regulated and finely tuned two-
76 way communication between the plastid and the nucleus, including both anterograde (nucleus-to-
77 plastid) and retrograde (plastid-to-nucleus) signaling. An increasing number of overlapping retrograde
78 signaling pathways, triggered by developmental or environmental defects in plastid function, have
79 been identified (Chan et al., 2015; Woodson and Chory, 2012). Numerous retrograde signals have
80 been proposed, including intermediates in tetrapyrrole (Mochizuki et al., 2001) or isoprenoid (Xiao et
81 al., 2012) biosynthesis, heme (Woodson et al., 2011), phosphonucleotides (Estavillo et al., 2011),
82 reactive oxygen species (ROS) (Wagner et al., 2004) and oxidized carotenoids (Ramel et al., 2012).
83 Despite the diversity, all these pathways and signals link a disruption in plastid homeostasis to altered
84 nuclear gene expression (Chan et al., 2015).
85
86 One retrograde signaling pathway that may serve to connect plastid signals to shoot development is
87 the GENOMES UNCOUPLED (GUN1) / ABA-INSENSITIVE 4 (ABI4) pathway (Fernandez and Strand,
88 2008; Leon et al., 2012). ABI4 is a nuclear transcription factor involved in many plant developmental
89 pathways, including response to ABA, sugar signaling, and mitochondrial retrograde signaling (Leon et
90 al., 2012). GUN1 is a plastid protein of unclear molecular function thought to function with ABI4 in at
91 least two retrograde signaling pathways, one that coordinates plastid and nuclear gene expression
92 during development, and one that respond to defects in chlorophyll biosynthesis (Cottage et al., 2010;
93 Koussevitzky et al., 2007; Sun et al., 2011).
94
95 ROS are both byproducts of the metabolic reactions that occur within cells, and serve as important
96 signaling molecules in plant development, stress response, and programmed cell death (Apel and Hirt,
97 2004). In plant cells, chloroplasts are major sources of ROS such as singlet oxygen ($^1O_2$), superoxide
98 (O_2^-), and hydrogen peroxide (H_2O_2). Numerous studies support a role for ROS in retrograde signaling

99 (Barajas-Lopez Jde et al., 2013; Galvez-Valdivieso and Mullineaux, 2010; Pogson et al., 2008) and
100 their involvement in multiple pathways including the GUN1/ABI4 pathway (Moulin et al., 2008).
101
102 We have been using an Arabidopsis mutant with constitutively osmotically stressed plastids (*msl2*
103 *msl3* (Veley et al., 2012)) as a model system to address the developmental effects of plastid
104 dysfunction. MSL2 and MSL3 are two members of the MscS-Like family of mechanosensitive ion
105 channels that localize to the plastid envelope and are required for normal plastid size, shape, and
106 division site selection (Haswell and Meyerowitz, 2006; Wilson et al., 2011). By analogy to family
107 members in bacteria (Levina et al., 1999) and plants (Hamilton et al., 2015), and based on *in vivo*
108 experiments (Veley et al., 2012), MSL2 and MSL3 are likely to serve as osmotic "safety valves",
109 allowing plastids to continuously maintain osmotic homeostasis during normal growth and
110 development. In addition, *msl2 msl3* mutant plants exhibit small stature, variegated leaf color, and
111 ruffled leaf margins. These whole-plant defects can be attributed to plastid osmotic stress, as they are
112 suppressed by environmental and genetic manipulations that increase cytoplasmic osmolarity and
113 draw water out of the plastid (Veley et al., 2012; Wilson et al., 2014).
114
115 Here we report a new and unexpected phenotype associated with *msl2 msl3* mutants, and establish
116 the molecular and genetic pathways that underlie it. Our data provide evidence that plastid status is
117 important to maintain cell identity decisions at the SAM, that plastid dysfunction promotes cell
118 proliferation through two non-redundant pathways: one involving SAM identity genes and CK; and one
119 involving the production of plastidic ROS, ABA, and the GUN1/ABI4 pathway.
120

121 **RESULTS**

122

123 ***msl2 msl3* double mutants develop callus at the shoot apex**

124

125 When grown on solid media, *msl2 msl3* double mutant plants developed a proliferating mass of
126 undifferentiated cells, or callus, at the apex of the plant (Fig. 1A-D). Calluses lacked pigmentation and
127 formed translucent finger-like cellular projections across their surface. A single mass at the center of
128 the apex, twin masses associated with the cotyledon petioles; and occasionally three masses were
129 observed Fig. 1A-C). New green tissue was frequently observed growing out of the apical callus (white
130 arrow, Fig. 1D).

131

132 We characterized the developmental progression of callus production in *msl2 msl3* seedlings, starting
133 at 8 days after germination (DAG) and ending at 22 DAG for the mutant and at 16 DAG (when
134 seedlings bolted) for the wild type (Fig. 1E, top two rows). Masses of callus tissue were apparent to
135 the naked eye at the apex of *msl2 msl3* seedlings between 14 and 16 DAG and continued to grow in
136 size through 22 DAG. The percent of *msl2 msl3* seedlings with callus increased to ~82% by 21 DAG
137 (Fig. 1F); callus was not observed in any wild type plants at any developmental stage. To determine
138 how suppression of developmental defects depended on age and developmental stage, seedlings
139 were germinated on MS solid media and transferred to media containing 100 mM NaCl at 2, 5, 7, or 9
140 DAG and assessed at 21 DAG for callus formation and leaf development. Full suppression of callus
141 formation and abnormal leaf development was only observed in seedlings transferred to solid media
142 containing NaCl from MS at 2 DAG (Fig. 1G and H). The reason for a slight reduction in callus
143 formation was observed in seedlings transferred from MS to MS at later stages of development is
144 unclear. These results establish a small developmental window, after which alleviation of plastid
145 hypoosmotic stress can no longer suppress leaf morphology defects and apical callus production in
146 *msl2 msl3* mutants.

147

148 The converse experiment was also conducted, in which seedlings were germinated on solid media
149 containing 82 mM NaCl and then transferred to media lacking NaCl (Fig. 1H and S1). Seedlings that
150 were transferred to NaCl-free media at 7 and 9 DAG had wild-type true leaves and lacked apical callus,
151 but after transfer developed leaves that exhibited the usual mutant phenotypes (Fig. S1). These
152 observations show that plastid osmotic homoeostasis is continuously required to maintain normal leaf
153 development.

154

155 **Plastids in the SAM of *msl2 msl3* mutants are morphologically abnormal**

156

157 We next characterized the morphology of developing chloroplasts and proplastids in the SAM and
158 surrounding tissue of *msl2 msl3* mutant seedlings using transmission electron microscopy (Fig. 2A
159 and S2B). In the *msl2 msl3* mutant, young chloroplasts were enlarged, lacked the lens shape of wild-
160 type chloroplasts, and exhibited a disorganized developing thylakoid network (Fig. 2B-C). In
161 agreement with previous reports (Charuvi et al., 2012), wild-type proplastids appeared as small
162 structures (0.5-1 μm in diameter) containing rudimentary thylakoid networks of varying developmental
163 stages, plastoglobules, and double membranes (Fig. 2F and Fig. S2A). However, in the SAM of *msl2*
164 *msl3* mutants, entities with these established features had decreased stromal density and were greatly
165 enlarged compared to the wild type (asterisks in Fig. 2A and S2B, Fig. 2D). Many exceeded 5 μm in
166 diameter. All were clearly bound by a double membrane (white arrow, Fig. 2E and S2C-D). These data
167 show that the greatly enlarged phenotype of non-green plastids of the leaf epidermis (Haswell and
168 Meyerowitz, 2006; Veley et al., 2012) extends to proplastids of the SAM.

169

170 **MSL2 function is required in the SAM or leaf primordia to prevent callus production**

171

172 To determine if MSL2 expression in the SAM and leaf primordia was required to prevent callus
173 production in the *msl2 msl3* background, we examined apical callus production in *msl2 msl3* mutant
174 plants expressing *MSL2* from the *SCARECROW (SCR)* promoter, which is expressed throughout the
175 L1 cell layer of the meristem including the PZ and in most cells of leaf primordia (Wysocka-Diller et al.,
176 2000). As shown in Fig. 2G, apical callus formation was fully suppressed in T2 *msl2 msl3 SCRpMSL2*
177 lines. While these plants developed multiple sets of developmentally normal true leaves, the majority
178 of T2 lines examined exhibited reduced stature. Thus, expression of *MSL2* in the L1 cell layer of the
179 SAM and leaf primordia is sufficient to prevent callus formation and partially suppress other aerial
180 tissue phenotypes.

181

182 **Callus produced in *msl2 msl3* mutants is the result of an altered cytokinin: auxin ratio and**
183 **requires CK perception**

184

185 The production of shooty callus has been associated with increased production or availability of CKs
186 and an imbalance in the cytokinin: auxin ratio (Frank et al., 2002; Frank et al., 2000; Lee et al., 2004).
187 Consistent with these observations, apical callus production, dwarfing and leaf phenotypes of the *msl2*
188 *msl3* double mutant were strongly suppressed when seedlings were grown on media supplemented

189 with the synthetic auxin 1-naphthaleneacetic acid (NAA) (Fig. 3A, C). When *msl2 msl3* seedlings
190 harboring the plastid marker RecA-dsRED (Haswell and Meyerowitz, 2006; Wilson et al., 2014) were
191 grown on 2 μM NAA, no change in the large, round non-green plastid phenotype was observed (Fig.
192 3B), indicating that NAA treatment suppresses callus formation downstream of effects on plastid
193 morphology. In agreement with previous data, growth on media supplemented with osmolytes fully
194 suppressed the plastid morphology defects (Veley et al., 2012). We next measured the CK and auxin
195 levels present in 21-day-old wild type and mutant seedlings by liquid chromatography-mass
196 spectrometry/mass spectrometry. Trans-Zeatin-riboside levels were increased ~6.5-fold in *msl2 msl3*
197 mutant seedlings compared to the wild type, but IAA levels were not significantly changed (Fig. 3D).
198
199 The *ARABIDOPSIS HISTIDINE KINASE (AHK)2* gene encodes one of three related histidine kinases
200 known to function as CK receptors in Arabidopsis (Ueguchi et al., 2001; Yamada et al., 2001), and an
201 *AHK2* loss of function mutant, *ahk2-2* (Higuchi et al., 2004) is impaired in CK-induced up-regulation of
202 *WUS* (Gordon et al., 2009). Two independently isolated *msl2 msl3 ahk2-2* triple mutants were similar
203 to the msl2 msl3 double with respect to leaf developmental defect (Fig. 3E), but showed a significant
204 reduction in apical callus formation with less than 40% of seedlings developing callus (Fig. 3F).
205 Incomplete suppression with respect to callus formation may be due to redundancy among CK
206 receptors (Gordon et al., 2009).
207
208 To determine if feedback loops involving *WUS*, *ARRs* (Gordon et al., 2009; Schuster et al., 2014), or
209 the meristem identity gene *STM* (Scofield et al., 2013) were mis-regulated in *msl2 msl3* seedlings,
210 Quantitative RT-PCR was used to determine transcript levels in the aerial tissue of 7- and 21-day-old
211 seedlings (Fig. 3G). In *msl2 msl3* mutant seedlings *WUS* transcript levels were up-regulated 5.3-fold
212 compared to the wild type by 7 DAG (prior to visible callus development, Fig. 1E); and 4-fold by 21
213 DAG. *STM* expression levels were up-regulated 2.1-fold in 7-day-old *msl2 msl3* mutants, but were not
214 distinguishable from the wild type at 21 DAG. *ARR7* and *ARR15* transcript levels were reduced in both
215 7 and 21 day old *msl2 msl3* mutant seedlings compared to wild type, exhibiting 2 to 2.6-fold and 3- to
216 6-fold decreases, respectively. Transcriptional repression is specific to *ARR7* and *ARR15*, as
217 transcript levels of two other A-type *ARR* genes were either unchanged (*ARR4*) or slightly elevated
218 (*ARR5*) in *msl2 msl3* mutant seedlings compared to wild type.
219
220 **Preventing Pro biosynthesis results in a dramatic increase in callus formation and CK levels in**
221 **the *msl2 msl3* background**
222

223 It was not obvious how the constitutive plastid osmotic stress experienced by *msl2 msl3* mutants might
224 elicit these effects, but we reasoned that the hyper-accumulation of solutes previously observed in
225 *msl2 msl3* mutants, especially the compatible osmolyte Proline (Pro) (Wilson et al., 2014), might be
226 responsible. To test this hypothesis, we crossed the *pyrroline-5-carboxylate synthetase1-1* (*p5cs1-4*)
227 lesion into the *msl2 msl3* mutant background. P5CS1 catalyzes the primary step in the inducible
228 production of Pro (Verslues and Sharma, 2010), and stress-induced Pro levels are low in this mutant
229 (Szekely et al., 2008). *msl2 msl3 p5cs1-4* triple mutant seedlings exhibited larger calluses than the
230 *msl2 msl3* double, frequently forming multiple calluses (Figs. 1E, and S3A), and formation was more
231 observed at earlier stages of development in *msl2 msl3 p5cs1-4* triple compared to *msl2 msl3* double
232 mutants (Fig. 4A, light blue bars)—at 14 DAG over 40% of triple mutant seedlings had visible callus,
233 while only 15% of the double *msl2 msl3* mutants did (Fig. 4A, light blue bars). Neither wild type nor
234 *p5cs1-4* single mutants produced callus at any time point. A different mutant allele of *P5CS1*, *p5cs1-1*
235 (Szekely et al., 2008), also enhanced callus formation in the *msl2 msl3* background (Fig. S3B-C). In
236 addition *msl2 msl3 p5cs1-4* triple mutants exhibited 7 times more trans-Zeatin-riboside levels than
237 *msl2 msl3* mutants (Fig. 3D). Supplementing growth media had no effect on callus production in *msl2*
238 *msl3* double or *msl2 msl3 p5cs1-4* triple mutants at any time point (Fig. 4A), even though *msl2 msl3*
239 *p5cs1-4* triple mutant seedlings grown on 20 mM Pro for 21 DAG contained as much Pro as the *msl2*
240 *msl3* double (Fig. 4B).
241
242 The process of Pro biosynthesis is a key reductive pathway that helps maintain cellular redox
243 homeostasis (Szabados and Savoure, 2010), and could function to reduce callus production in the
244 *msl2 msl3* mutant background if ROS accumulation were involved. To characterize the levels and
245 localization of ROS in *msl2 msl3* double and *msl2 msl3 p5cs1-4* triple mutants, 7-, 14-, and 21-day-old
246 mutant and wild-type seedlings were stained with 3, 3 diaminobenzidine (DAB) to detect hydrogen
247 peroxide (H_2O_2) or nitroblue tetrazolium (NBT) to detect superoxide (O_2^-) (Fig. 4C). Both double and
248 triple mutants accumulated high levels of H_2O_2 and O_2^- in the SAM region relative to the *p5cs1-4* single
249 mutant or the wild type. Precipitate was visible earlier in the *msl2 msl3 p5cs1-4* triple mutant (by 14
250 DAG compared to 21 DAG in the in the double *msl2 msl3* mutant). Quantitation of H_2O_2 levels using
251 an Amplex Red enzyme assay at these same time points showed consistent accumulation of H_2O_2 in
252 the double and triple mutants, rising to nearly three-fold over wild type by 21 DAG (Fig. 4D). Levels of
253 formazan, the product of NBT reduction by O_2^-, increased in *msl2 msl3* and *msl2 msl3 p5cs1-4* to
254 more than 2.5-fold above wild-type levels at 21 DAG (Fig. 4E). Calluses generated by incubating
255 *Arabidopsis thaliana* Col-*0* root explants on Callus Inducing Media also showed strong NBT staining in

256 areas of cell proliferation (Fig. S4), providing evidence that ROS accumulation may be a general
257 feature of callus tissue (Lee et al., 2004).
258
259 **The accumulation of superoxide in response to plastid hypo-osmotic stress is required for**
260 **callus formation in the *msl2 msl3* background.**
261
262 In plastids, the photoreduction of molecular O_2 generates O_2^-, which is then rapidly converted into
263 H_2O_2 by plastid-localized superoxide dismutase enzymes (Asada, 2006). To determine if plastid
264 osmotic stress and the accumulation of O_2^- at the apex of *msl2 msl3* double and *msl2 msl3 p5cs1-4*
265 triple mutants play causative roles in callus formation, plants were germinated on or transferred to
266 solid media supplemented with 82 mM NaCl or with TEMPOL (a O_2^- scavenger) at 3 or 7 DAG and
267 stained with NBT at 21 DAG. Growth on media containing NaCl suppressed O_2^- accumulation in *msl2*
268 *msl3* double and *msl2 msl3 p5cs1-4* triple mutant seedlings (Fig. 5A), completely prevented callus
269 formation (Fig. 5B), suppressed defects in non-green plastid morphology (Fig. 5C) and leaf
270 morphology (Fig. 5A). Thus, plastid osmotic stress is responsible for O_2^- accumulation as well as callus
271 formation in *msl2 msl3* and *msl2 msl3 p5cs1-4* mutants. Consistent with Fig. 1H, growth on NaCl
272 suppressed callus formation and ROS accumulation only if supplied prior to 7 DAG.
273
274 Growth on TEMPOL-containing media successfully prevented the accumulation of O_2^- in the SAM of
275 *msl2 msl3* and *msl2 msl3 p5cs1-4* mutants, regardless of seedling age at time of application (Fig. 5A),
276 but did not affect plastid morphology (Fig, 5C) nor leaf morphology defects (Fig. 5A). Treating double
277 and triple mutant seedlings with TEMPOL at all developmental stages partially suppressed callus
278 formation (Fig. 5C). Less than 40% of double mutant seedlings exhibited apical calluses when grown
279 in the presence of TEMPOL, compared to > 90% when grown on MS without TEMPOL. TEMPOL-
280 mediated callus suppression is thus independent or downstream of the developmental window in
281 which addition of osmotic support must be provide for complete suppression of aerial phenotypes
282 (Figs 1H and 5A-B).
283
284 A complementary genetic approach to suppressing O_2^- accumulation in the plastid was taken by over-
285 expressing wild type or miR398-resistant forms of the chloroplast-localized Cu/Zn Superoxide
286 Dismutase CSD2 (Kliebenstein et al., 1998; Sunkar et al., 2006) in the *msl2 msl3* mutant background.
287 The percentage of seedlings with visible apical callus at 21 DAG was decreased to 50% or less in six
288 independent T2 lines segregating either wild-type (*CSD2*, lines #2, #4, and #7) or miR398 resistant
289 (*mCSD2*, lines #1, #3, #5) *CSD2* over-expression constructs (Fig. 5D). Approximately 50% of T2

290 seedlings showed strong O_2^- accumulation by NBT staining, which was localized to developing callus,
291 compared to 90% of *msl2 msl3* seedlings (Fig. 5E). 15-30% of seedlings in the CDS2 over-expression
292 lines exhibited both low levels of O_2^- accumulation at their shoot apex and did not develop callus; less
293 than 5% of *msl2 msl3* seedlings had these characteristics. Over-expression of *CSD2* did not suppress
294 abnormal leaf development (Fig. 5F).
295
296 **Callus production requires ABA biosynthesis, ABI4 and GUN1**
297
298 As *msl2 msl3* double mutants exhibit increased levels of ABA and up-regulation of ABA biosynthesis
299 genes (Wilson et al., 2014), we hypothesized that a pathway involving the hormone ABA and the
300 GUN1 and ABI4 gene products might account for the pleiotropic defects in the *msl2 msl3* mutant
301 (Koussevitzky et al., 2007; Zhang et al., 2013). Indeed, callus formation and leaf development defects
302 were strongly suppressed in the triple mutant, with only ~20% of *msl2 msl3 aba2-1* seedlings
303 developing callus at the shoot apex by 21 DAG (Fig. 6A, B). Similar suppression of *msl2 msl3* aerial
304 defects was observed in four other independently isolated *msl2 msl3 aba2-1* triple mutant lines. The
305 *msl2 msl3 aba2-1* triple mutant accumulated trans-Zeatin-riboside to levels similar to the *msl2 msl3*
306 double mutant (Fig. 3D), suggesting that ABA and CK promote callus formation through independent
307 pathways.
308
309 To test if GUN1 is involved in the perception of signals generated by plastid osmotic stress, we
310 crossed the *gun1-9* (Koussevitzky et al., 2007) allele into the *msl2 msl3* mutant background and
311 analyzed the offspring of a single *msl2 msl3 gun1-2 (+/-)* mutant plant. Out of 30 seedlings, 7
312 triple *msl2 msl3 gun1-9* seedlings were identified by PCR genotyping. None of the seven seedlings
313 formed apical callus when grown on solid media, whereas sibling *msl2 msl3 gun1-9* (+/-) seedlings
314 were indistinguishable from *msl2 msl3* double mutants (Fig. 6C). In addition, all seven *msl2 msl3*
315 *gun1-9* triple mutant siblings produced larger, greener, and more normally shaped true leaves than
316 their *msl2 msl3* and *msl2 msl3 gun1-9+/1* siblings.
317
318 The strong *abi4-1* allele (Finkelstein et al., 1998) was also introduced into the *msl2 msl3* background,
319 and *msl2 msl3 abi4-1* mutants also exhibited reduced apical callus formation; only ~26% of *msl2 msl3*
320 *abi4-1* seedlings from two independently isolated lines developed callus (Fig. 6B). Neither leaf
321 developmental defects nor ROS accumulation was suppressed in the *msl2 msl3 abi4-1* mutant, and
322 *msl2 msl3 abi4-1* seedlings stained with DAB or NBT showed a pattern of ROS accumulation similar
323 to the *msl2 msl3* double mutant (Fig. 6D, E). These staining patterns were not observed in wild type or

324 *abi4-1* single mutants. These results are consistent with a model wherein ABI4 functions downstream
325 of ROS accumulation, and likely in a pathway with GUN1, to induce apical callus formation in
326 response to plastid osmotic stress.
327

328 **DISCUSSION**

329

330 One of the most fundamental decisions a cell can make is whether to proliferate or to differentiate. In
331 the plant SAM, this decision must be spatially and temporally controlled, so that cells remain in an
332 undifferentiated, pluripotent state in the central zone of the meristem and then differentiate properly as
333 they are recruited into organs at the PZ. Here we use the *msl2 msl3* mutant as a model system to
334 show that, in the Arabidopsis SAM, proliferation versus differentiation signals are coordinated not only
335 at the tissue- and cellular-level, but also at the organellar level. We further applied genetic, molecular,
336 biochemical, and pharmacological approaches to identify two non-redundant pathways through which
337 plastid dysfunction produces apical callus (illustrated in Fig. 7).

338

339 **Plastid dysfunction results in the production of callus at the plant SAM**

340

341 Plants lacking functional versions of the mechanosensitive ion channel homologs MSL2 and MSL3
342 robustly produce callus tissue at the apex of the plant when grown on solid media (Fig. 1). Of the large
343 number of previously described mutants that produce callus (Ikeuchi et al., 2013), the *msl2 msl3*
344 mutant most closely resembles plants silenced for the cell cycle inhibitor genes *KIP-RELATED*
345 *PROTEIN (KRP)* (Anzola et al., 2010), the *main-like1 (mail1)* mutant when grown on sucrose (Uhlken
346 et al., 2014), and the *N-isobutyl decanamide-hypersensitive (dhm1)* mutant (Pelagio-Flores et al.,
347 2013). Molecular complementation with *MSL2* under the control of the *SCARECROW* promoter
348 established that MSL2/MSL3 are required only in the L1 layer of the CZ and/or PZ of the SAM to
349 prevent callus formation (Fig. 2G) and that their function is critical during the first 5 days after
350 germination (Fig 1G, H). The production of apical callus in the *msl2 msl3* mutant is associated with
351 dramatically enlarged and developmentally abnormal plastids specifically in the SAM (Fig. 2A-F, S2A-
352 D). Developmentally defective plastids were also observed in the SAM of another apical callus-
353 producing mutant, *tumorous shoot development (tsd)1* (Frank et al., 2002).

354

355 **Disrupting the CK/WUS feedback loop in the SAM leads to increased proliferation and the**
356 **production of callus**

357

358 *msl2 msl3* mutants exhibit several previously established hallmarks of increased proliferation at the
359 SAM, including increased levels of CK< up-regulation of the stem cell identity gene *WUSCHEL*, and
360 down-regulation of CK signaling inhibitors (Fig. 3D, G), suggesting that plastid osmotic stress activates
361 the CK/WUS feedback loop (Gaillochet et al., 2015) (top pathway, Fig. 7). The resulting imbalance in

362 the cytokinin: auxin ratio is likely to underlie callus formation in the *msl2 msl3* background, as
363 supplementing seedlings with exogenous auxin robustly suppresses all mutant phenotypes (Fig. 3A,
364 C) without affecting plastid osmotic stress (Fig 3B). In addition, the CK receptor AHK2 is required for
365 efficient callus formation (Fig. 3E, F). *AHK2* is required to maintain WUS expression in the meristem in
366 response to CK treatment in the CK/WUS feedback loop (Gordon et al., 2009).
367
368 Several previously identified callus-producing mutants in Arabidopsis and Helianthus also exhibit both
369 up-regulated CK signaling and defects in meristem identity gene expression, including *tsd1* (Frank et
370 al., 2002; Krupkova and Schmulling, 2009); EMB-2 (Chiappetta et al., 2006); and the *pasticcino*
371 mutants (Faure et al., 1998; Harrar et al., 2003). These data suggest that, rather than being
372 independent mechanisms for callus production (Ikeuchi et al., 2013), the CK-induced pathway and the
373 meristematic identity pathway are interconnected. Furthermore, the *msl2 msl3* double mutant is the
374 only callus-producing mutant identified to date with a primary defect in plastid-localized proteins,
375 adding a novel regulatory aspect to these known pathways, and providing the first functional link
376 between the CK/WUS regulatory loop and plastid retrograde signaling.
377
378 **Plastid retrograde signaling is required for increased proliferation and the production of callus**
379
380 Genetic lesions that reduce Pro biosynthesis significantly exacerbated callus production in the *msl2*
381 *msl3* background, an effect that can not be attributed to low levels of Pro itself (Figs. 1E, 4A, B, S3).
382 Instead, the hyper-accumulation of ROS that results from blocking Pro biosynthesis is required (Fig. 5).
383 Treatment with exogenous ROS scavenger TEMPOL as well as over-production of CSD2, a
384 chloroplast-localized superoxide-scavenging enzyme, prevented or reduced callus formation. Plastid
385 osmotic stress was required for ROS hyper-accumulation (Fig. 5A-C). In addition, the analysis of
386 callus formation in higher order mutants established that ABA biosynthesis and the retrograde
387 signaling proteins GUN1 and ABI4 were required for callus formation and act downstream of ROS (Fig.
388 6, bottom pathway in Fig. 7). Because we were able to specifically suppress callus production, ROS
389 accumulation, and impaired leaf development by increasing cytoplasmic osmolarity in the *msl2 msl3*
390 background, this phenotype is very unlikely to be due to a loss of specific signaling by MSL2 or MSL3.
391
392 Multiple genetic links between plastid function and cell fate in the shoot have been previously
393 described, and are often cited as evidence for retrograde signaling (Inaba and Ito-Inaba, 2010; Lepisto
394 and Rintamaki, 2012; Lundquist et al., 2014). Whether ROS and/or the ABA/GUN1/ABI4 retrograde
395 signaling pathway are employed to communicate plastid dysfunction to shoot development in any of

396 these other mutants is not known. However, the application of pharmacological inhibitors of plastid
397 development or function was used to demonstrate that leaf adaxial/abaxial patterning is regulated by
398 plastid protein translation in a GUN1-dependent pathway (Tameshige et al., 2013), and the GUN1
399 pathway is required to facilitate the switch from leaf cell proliferation to expansion and differentiation
400 (Andriankaja et al., 2012). Taken together with the results reported here, these data support previously
401 proposed models wherein a variety of plastid dysfunctions are communicated to leaf development
402 through similar or overlapping pathways that include GUN1 (Koussevitzky et al., 2007; Leon et al.,
403 2012).
404
405 We note that only a few of the genetic or pharmacological treatments that suppressed callus formation
406 in the *msl2 msl3* mutant also suppressed the leaf developmental defects. Growth on exogenous auxin
407 was the only treatment to completely suppress all of the mutant phenotypes, while preventing ABA
408 biosynthesis, ROS accumulation or GUN1/ABI4 function only partially rescued leaf defects (Figs. 6A-
409 E). It is possible that these differences are due to genetic redundancy or to limited uptake or transport
410 of TEMPOL. Alternatively, there may be two fundamentally different processes that respond to plastid
411 osmotic stress in the *msl2 msl3* mutant: one that functions in the SAM during early development, and
412 one that functions later on in the leaves. In support of the latter proposal, subjecting seedlings to mild
413 hyperosmotic stress has been shown to prevent leaf cell proliferation (Skirycz et al., 2011).
414
415 ***msl2 msl3* mutants provide a functional link between the CK/WUS feedback loop and plastid**
416 **retrograde signaling in controlling cell fate at the plant apex.**
417
418 Our working model, illustrated in Fig. 7, is that the production of apical callus in *msl2 msl3* mutants
419 operates through two non-redundant pathways: the CK/WUS feedback loop and a retrograde signaling
420 pathway involving ROS, ABA, ABI4 and GUN1. While the data presented here establish that both of
421 these pathways are required for callus formation in the *msl2 msl3* background, whether they operate
422 completely independently or are interconnected is not yet clear. In Fig. 7, we present them as
423 separate pathways. Support for this comes from the fact that CK levels remain elevated in the *aba2*
424 *msl2 msl3* triple mutant (Fig. 3D), indicating that ABA biosynthesis is not upstream of the CK/WUS
425 feedback loop.
426
427 In addition to promoting meristem identity, CKs are implicated in various aspects of plastid function,
428 including plastid division and chlorophyll biosynthesis, often through modulating the expression of
429 nuclear-encoded plastid genes (Cortleven and Schmulling, 2015). Changes in CK levels in response

430 to environmental stresses known to affect chloroplast function such as drought, salinity, and
431 temperature extremes (Dobra et al., 2010; Kudoyarova et al., 2007; Nishiyama et al., 2011;
432 Pospisilova et al.) have been documented. Additionally, CKs have been shown to preserve chloroplast
433 integrity during leaf senescence by inducing protective antioxidant mechanisms (Prochazkova et al.,
434 2008). Recent work has even provided a link between CK signaling and high light-induced
435 photoinhibition (Cortleven et al., 2014). Thus, the work reported here contributes to a growing body of
436 research suggesting that CKs are involved in stress-response and retrograde signaling pathways.
437
438 We speculate that two-way communication between plastids and cell fate decisions is essential to
439 coordinate the developmental and functional state of the plastid with that of the cell within which it
440 resides, and that it therefore necessarily involves multiple pathways. These results add yet another
441 layer of complexity to the many regulatory pathways and feedback loops that govern dynamic cell
442 identity decision-making at the plant shoot apex, and provide a foundation for future investigation into
443 the relationship between meristem identity and plastid homeostasis in the SAM.
444

445 **MATERIALS AND METHODS**

446

447 **Arabidopsis (*Arabidopsis thaliana*) Mutants**

448 The *aba2-1* (CS156), *abi4-1* (CS8104), *p5cs1-4* (SALK_063517), *p5cs1-1* (SALK_058000), *ahk2-2*
449 (SALK_052531), *gun1-9*, and *msl2-3* alleles are in the Columbia-*0* background. The *msl3-1* allele is in
450 the Wassilewskija background (Haswell and Meyerowitz, 2006). Derived cleaved-amplified
451 polymorphic sequence genotyping (Neff et al., 1998) of the *gun1-9* allele was performed using oligos
452 CGAACGACGAAAGATTGTGAGGAGGGTCT and CCTGCAAGCATTCAGAATCGCTGAAAAAGG,
453 digesting with PstI. The *abi4-1* allele was similarly genotyped with oligos
454 TCAATCCGATTCCACCACCGAC and CCACTTCCTCCTTGTTCCTGC, digesting with NlaI. PCR
455 genotyping of *msl*, *p5cs1*, and *aba2-1* alleles was performed as described (Sharma and Verslues,
456 2010; Szekely et al., 2008; Wilson et al., 2011).

457

458 **Plant growth**

459 Plants were grown on full-strength Murashige and Skoog (MS) medium (pH 5.7; Caisson Labs) with
460 0.8% (w/v) agar (Caisson Labs). NaCl, L-Pro (Sigma) and TEMPOL (Sigma) were added before
461 autoclaving. For transfer assays, seed was surface-sterilized, sown on nylon mesh strips overlaid on
462 1X MS or 1X MS + 82 mM NaCl, and stratified for 2 d at 4°C before growth and transfer as described.
463 All plants were grown at 23°C under a 16 h light regime with light fluence from 130 to 160 μmol m^{-1} s^{-1}.

464

465 **Microscopy**

466 Confocal microscopy of ds-RED labeled non-green plastids was performed as in (Wilson et al., 2014).
467 Bright-field images were captured with an Olympus DP71 microscope digital camera and processed
468 with DP-BSW software. Transmission electron microscopy was done on thin sections of tissue fixed
469 for 2 h in 2% glutaraldehyde, post-fixed 90 minutes in 2% osmium tetroxide and embedded in Spurr's
470 resin. Sections were post stained in uranyl and lead salts.

471

472 **ROS detection and Quantification**

473 Detection of H_2O_2 using 3,3'-Diaminobenzidine (DAB, Sigma) was performed as described (Wu et al.,
474 2012) with the following modifications. Whole seedlings were incubated for 2 hrs in 1 mg/ml DAB prior
475 to vacuum infiltration, incubated in the dark for an additional 12 hrs, and then cleared with an ethanol
476 series. An Amplex Red Hydrogen Peroxide/Peroxidase Assay Kit (Invitrogen) was used to measure
477 H_2O_2 production in seedlings. For in vitro localization of O_2^- with Nitrotetrazolium Blue chloride (NBT;
478 Sigma), whole seedlings were vacuum-infiltrated with 0.1% (w/v) NBT in a 10 mM potassium

479 phosphate buffer (pH 7.8) containing 10 mM NaN_3. After 1 hour incubation in the dark at RT seedlings
480 were cleared with an ethanol series. Quantification of formazan levels was performed as described in
481 (Myouga et al., 2008).
482
483 **Hormone level measurements**
484 Approximately 100 mg of plant tissue was sampled for each of three replicates, frozen in N_2(l), and
485 stored at -80°C before being assayed. Hormone levels were quantified by liquid chromatography–
486 mass spectrometry/mass spectrometry as in (Chen et al., 2009).
487
488 **Subcloning and Transgenic lines**
489 pENTR-MSL2 (Haswell and Meyerowitz, 2006) was used in a Gateway technology (Life Technologies)
490 recombination reaction with pSCR:GW (Michniewicz et al., 2015) to create *pSCR:MSL2*.
491
492 **Quantitative Reverse Transcription-PCR**
493 Quantitative reverse transcription-PCR was performed as previously described (Wilson et al., 2011).
494 Primers used for gene expression analysis of *Actin* and *ARR* genes were previously described (Wilson
495 et al., 2014; Zhao et al., 2010). The following primer pairs were used to amplify *WUS*
496 (GCGATGCTTATCTGGAACAT and CTTCCAGATGGCACCACTAC) and *STM*
497 (CAAATGGCCTTACCCTTCG and GCCGTTTCCTCTGGTTTATG).
498
499 **Quantification of Free Pro**
500 Pro was assayed using a ninhydrin assay adapted to fit a 1.7-mL microcentrifuge tube format
501 (Abraham et al., 2010).
502
503 **ACKNOWLEDGEMENTS**
504 We thank the Washington University Plant Growth Facility staff, Kelsey Kropp, and Matt Mixdorf for
505 technical assistance. The Proteomics and Mass Spectrometry Facility of the Donald Danforth Plant
506 Science Center performed the hormone quantification. Lucia Strader provided *abi4-1* seeds and
507 pSCR:GW; Ramanjulu Sunkar provided pBIB-CSD2 and pBIB-mCSD2; and Jesse Woodson and
508 Joanne Chory provided *gun1-9* seeds.
509
510 **COMPETING INTERESTS**
511 No competing interests declared.
512

513 **AUTHOR CONTRIBUTIONS**

514 Study conception and manuscript preparation, MEW, ESH; conducting the research and formal
515 analysis, MEW, EHB; funding acquisition, ESH.

516

517 **REFERENCES**

518

519 **Abraham, E., Hourton-Cabassa, C., Erdei, L. and Szabados, L.** (2010). Methods for determination
520 of proline in plants. *Methods Mol Biol* **639**, 317-331.

521 **Aichinger, E., Kornet, N., Friedrich, T. and Laux, T.** (2012). Plant stem cell niches. *Annual review of*
522 *plant biology* **63**, 615-636.

523 **Andriankaja, M., Dhondt, S., De Bodt, S., Vanhaeren, H., Coppens, F., De Milde, L., Muhlenbock,**
524 **P., Skirycz, A., Gonzalez, N., Beemster, G. T., et al.** (2012). Exit from proliferation during leaf
525 development in Arabidopsis thaliana: a not-so-gradual process. *Developmental cell* **22**, 64-78.

526 **Anzola, J. M., Sieberer, T., Ortbauer, M., Butt, H., Korbei, B., Weinhofer, I., Mullner, A. E. and**
527 **Luschnig, C.** (2010). Putative Arabidopsis transcriptional adaptor protein (PROPORZ1) is
528 required to modulate histone acetylation in response to auxin. *Proceedings of the National*
529 *Academy of Sciences of the United States of America* **107**, 10308-10313.

530 **Apel, K. and Hirt, H.** (2004). Reactive oxygen species: metabolism, oxidative stress, and signal
531 transduction. *Annual review of plant biology* **55**, 373-399.

532 **Asada, K.** (2006). Production and scavenging of reactive oxygen species in chloroplasts and their
533 functions. *Plant physiology* **141**, 391-396.

534 **Barajas-Lopez Jde, D., Blanco, N. E. and Strand, A.** (2013). Plastid-to-nucleus communication,
535 signals controlling the running of the plant cell. *Biochimica et biophysica acta* **1833**, 425-437.

536 **Barton, M. K.** (2010). Twenty years on: the inner workings of the shoot apical meristem, a
537 developmental dynamo. *Dev Biol* **341**, 95-113.

538 **Chan, K. X., Phua, S. Y., Crisp, P., McQuinn, R. and Pogson, B. J.** (2015). Learning the Languages
539 of the Chloroplast: Retrograde Signaling and Beyond. *Annual review of plant biology*.

540 **Charuvi, D., Kiss, V., Nevo, R., Shimoni, E., Adam, Z. and Reich, Z.** (2012). Gain and loss of
541 photosynthetic membranes during plastid differentiation in the shoot apex of Arabidopsis. *The*
542 *Plant cell* **24**, 1143-1157.

543 **Chen, Q., Zhang, B., Hicks, L. M., Wang, S. and Jez, J. M.** (2009). A liquid chromatography-tandem
544 mass spectrometry-based assay for indole-3-acetic acid-amido synthetase. *Anal Biochem* **390**,
545 149-154.

546 **Chiappetta, A., Michelotti, V., Fambrini, M., Bruno, L., Salvini, M., Petrarulo, M., Azmi, A., Van**
547 **Onckelen, H., Pugliesi, C. and Bitonti, M. B.** (2006). Zeatin accumulation and misexpression
548 of a class I knox gene are intimately linked in the epiphyllous response of the interspecific
549 hybrid EMB-2 (Helianthus annuus x H. tuberosus). *Planta* **223**, 917-931.
550 **Chickarmane, V. S., Gordon, S. P., Tarr, P. T., Heisler, M. G. and Meyerowitz, E. M.** (2012).
551 Cytokinin signaling as a positional cue for patterning the apical-basal axis of the growing
552 Arabidopsis shoot meristem. *Proceedings of the National Academy of Sciences of the United*
553 *States of America* **109**, 4002-4007.
554 **Cortleven, A., Nitschke, S., Klaumunzer, M., Abdelgawad, H., Asard, H., Grimm, B., Riefler, M.**
555 **and Schmulling, T.** (2014). A novel protective function for cytokinin in the light stress
556 response is mediated by the Arabidopsis histidine kinase2 and Arabidopsis histidine kinase3
557 receptors. *Plant physiology* **164**, 1470-1483.
558 **Cortleven, A. and Schmulling, T.** (2015). Regulation of chloroplast development and function by
559 cytokinin. *Journal of experimental botany* **66**, 4999-5013.
560 **Cottage, A., Mott, E. K., Kempster, J. A. and Gray, J. C.** (2010). The Arabidopsis plastid-signalling
561 mutant gun1 (genomes uncoupled1) shows altered sensitivity to sucrose and abscisic acid and
562 alterations in early seedling development. *Journal of experimental botany* **61**, 3773-3786.
563 **Dobra, J., Motyka, V., Dobrev, P., Malbeck, J., Prasil, I. T., Haisel, D., Gaudinova, A., Havlova, M.,**
564 **Gubis, J. and Vankova, R.** (2010). Comparison of hormonal responses to heat, drought and
565 combined stress in tobacco plants with elevated proline content. *J Plant Physiol* **167**, 1360-
566 1370.
567 **Endrizzi, K., Moussian, B., Haecker, A., Levin, J. Z. and Laux, T.** (1996). The SHOOT
568 MERISTEMLESS gene is required for maintenance of undifferentiated cells in Arabidopsis
569 shoot and floral meristems and acts at a different regulatory level than the meristem genes
570 WUSCHEL and ZWILLE. *The Plant journal : for cell and molecular biology* **10**, 967-979.
571 **Estavillo, G. M., Crisp, P. A., Pornsiriwong, W., Wirtz, M., Collinge, D., Carrie, C., Giraud, E.,**
572 **Whelan, J., David, P., Javot, H., et al.** (2011). Evidence for a SAL1-PAP chloroplast
573 retrograde pathway that functions in drought and high light signaling in Arabidopsis. *The Plant*
574 *cell* **23**, 3992-4012.
575 **Faure, J. D., Vittorioso, P., Santoni, V., Fraisier, V., Prinsen, E., Barlier, I., Van Onckelen, H.,**
576 **Caboche, M. and Bellini, C.** (1998). The PASTICCINO genes of Arabidopsis thaliana are
577 involved in the control of cell division and differentiation. *Development* **125**, 909-918.
578 **Fernandez, A. P. and Strand, A.** (2008). Retrograde signaling and plant stress: plastid signals initiate
579 cellular stress responses. *Curr Opin Plant Biol* **11**, 509-513.

580 **Finkelstein, R. R., Wang, M. L., Lynch, T. J., Rao, S. and Goodman, H. M.** (1998). The Arabidopsis
581 abscisic acid response locus ABI4 encodes an APETALA 2 domain protein. *The Plant cell* **10**,
582 1043-1054.
583 **Fletcher, J. C., Brand, U., Running, M. P., Simon, R. and Meyerowitz, E. M.** (1999). Signaling of
584 cell fate decisions by CLAVATA3 in Arabidopsis shoot meristems. *Science* **283**, 1911-1914.
585 **Frank, M., Guivarc'h, A., Krupkova, E., Lorenz-Meyer, I., Chriqui, D. and Schmulling, T.** (2002).
586 Tumorous shoot development (TSD) genes are required for co-ordinated plant shoot
587 development. *The Plant journal : for cell and molecular biology* **29**, 73-85.
588 **Frank, M., Rupp, H. M., Prinsen, E., Motyka, V., Van Onckelen, H. and Schmulling, T.** (2000).
589 Hormone autotrophic growth and differentiation identifies mutant lines of Arabidopsis with
590 altered cytokinin and auxin content or signaling. *Plant physiology* **122**, 721-729.
591 **Gaillochet, C., Daum, G. and Lohmann, J. U.** (2015). O cell, where art thou? The mechanisms of
592 shoot meristem patterning. *Curr Opin Plant Biol* **23**, 91-97.
593 **Gaillochet, C. and Lohmann, J. U.** (2015). The never-ending story: from pluripotency to plant
594 developmental plasticity. *Development* **142**, 2237-2249.
595 **Galvez-Valdivieso, G. and Mullineaux, P. M.** (2010). The role of reactive oxygen species in
596 signalling from chloroplasts to the nucleus. *Physiologia plantarum* **138**, 430-439.
597 **Gordon, S. P., Chickarmane, V. S., Ohno, C. and Meyerowitz, E. M.** (2009). Multiple feedback
598 loops through cytokinin signaling control stem cell number within the Arabidopsis shoot
599 meristem. *Proceedings of the National Academy of Sciences of the United States of America*
600 **106**, 16529-16534.
601 **Hamilton, E. S., Jensen, G. S., Maksaev, G., Katims, A., Sherp, A. M. and Haswell, E. S.** (2015).
602 Mechanosensitive channel MSL8 regulates osmotic forces during pollen hydration and
603 germination. *Science* **350**, 438-441.
604 **Harrar, Y., Bellec, Y., Bellini, C. and Faure, J. D.** (2003). Hormonal control of cell proliferation
605 requires PASTICCINO genes. *Plant physiology* **132**, 1217-1227.
606 **Haswell, E. S. and Meyerowitz, E. M.** (2006). MscS-like proteins control plastid size and shape in
607 Arabidopsis thaliana. *Current biology : CB* **16**, 1-11.
608 **Higuchi, M., Pischke, M. S., Mahonen, A. P., Miyawaki, K., Hashimoto, Y., Seki, M., Kobayashi,**
609 **M., Shinozaki, K., Kato, T., Tabata, S., et al.** (2004). In planta functions of the Arabidopsis
610 cytokinin receptor family. *Proceedings of the National Academy of Sciences of the United*
611 *States of America* **101**, 8821-8826.
612 **Ikeuchi, M., Sugimoto, K. and Iwase, A.** (2013). Plant callus: mechanisms of induction and
613 repression. *The Plant cell* **25**, 3159-3173.

614 **Inaba, T. and Ito-Inaba, Y.** (2010). Versatile roles of plastids in plant growth and development. *Plant*
615 *& cell physiology* **51**, 1847-1853.
616 **Jarvis, P. and Lopez-Juez, E.** (2013). Biogenesis and homeostasis of chloroplasts and other plastids.
617 *Nature reviews. Molecular cell biology* **14**, 787-802.
618 **Kliebenstein, D. J., Monde, R. A. and Last, R. L.** (1998). Superoxide dismutase in Arabidopsis: an
619 eclectic enzyme family with disparate regulation and protein localization. *Plant physiology* **118**,
620 637-650.
621 **Koussevitzky, S., Nott, A., Mockler, T. C., Hong, F., Sachetto-Martins, G., Surpin, M., Lim, J.,**
622 **Mittler, R. and Chory, J.** (2007). Signals from chloroplasts converge to regulate nuclear gene
623 expression. *Science* **316**, 715-719.
624 **Krupkova, E. and Schmulling, T.** (2009). Developmental consequences of the tumorous shoot
625 development1 mutation, a novel allele of the cellulose-synthesizing KORRIGAN1 gene. *Plant*
626 *molecular biology* **71**, 641-655.
627 **Kudoyarova, G. R., Vysotskaya, L. B., Cherkozyanova, A. and Dodd, I. C.** (2007). Effect of partial
628 rootzone drying on the concentration of zeatin-type cytokinins in tomato (Solanum
629 lycopersicum L.) xylem sap and leaves. *Journal of experimental botany* **58**, 161-168.
630 **Larkin, R. M.** (2014). Influence of plastids on light signalling and development. *Philosophical*
631 *transactions of the Royal Society of London. Series B, Biological sciences* **369**, 20130232.
632 **Lee, J. H., Kim, D. M., Lim, Y. P. and Pai, H. S.** (2004). The shooty callus induced by suppression of
633 tobacco CHRK1 receptor-like kinase is a phenocopy of the tobacco genetic tumor. *Plant Cell*
634 *Rep* **23**, 397-403.
635 **Leibfried, A., To, J. P., Busch, W., Stehling, S., Kehle, A., Demar, M., Kieber, J. J. and Lohmann,**
636 **J. U.** (2005). WUSCHEL controls meristem function by direct regulation of cytokinin-inducible
637 response regulators. *Nature* **438**, 1172-1175.
638 **Leon, P., Gregorio, J. and Cordoba, E.** (2012). ABI4 and its role in chloroplast retrograde
639 communication. *Frontiers in plant science* **3**, 304.
640 **Lepisto, A. and Rintamaki, E.** (2012). Coordination of plastid and light signaling pathways upon
641 development of Arabidopsis leaves under various photoperiods. *Molecular plant* **5**, 799-816.
642 **Levina, N., Totemeyer, S., Stokes, N. R., Louis, P., Jones, M. A. and Booth, I. R.** (1999).
643 Protection of Escherichia coli cells against extreme turgor by activation of MscS and MscL
644 mechanosensitive channels: identification of genes required for MscS activity. *The EMBO*
645 *journal* **18**, 1730-1737.
646 **Long, J. A., Moan, E. I., Medford, J. I. and Barton, M. K.** (1996). A member of the KNOTTED class
647 of homeodomain proteins encoded by the STM gene of Arabidopsis. *Nature* **379**, 66-69.

648 **Luesse, D. R., Wilson, M. E. and Haswell, E. S.** (2015). RNA Sequencing Analysis of the msl2msl3,
649 crl, and ggps1 Mutants Indicates that Diverse Sources of Plastid Dysfunction Do Not Alter Leaf
650 Morphology Through a Common Signaling Pathway. *Frontiers in plant science* **6**, 1148.
651 **Lundquist, P. K., Rosar, C., Brautigam, A. and Weber, A. P.** (2014). Plastid signals and the bundle
652 sheath: mesophyll development in reticulate mutants. *Molecular plant* **7**, 14-29.
653 **Michniewicz, M., Frick, E. M. and Strader, L. C.** (2015). Gateway-compatible tissue-specific vectors
654 for plant transformation. *BMC Res Notes* **8**, 63.
655 **Mochizuki, N., Brusslan, J. A., Larkin, R., Nagatani, A. and Chory, J.** (2001). Arabidopsis genomes
656 uncoupled 5 (GUN5) mutant reveals the involvement of Mg-chelatase H subunit in plastid-to-
657 nucleus signal transduction. *Proceedings of the National Academy of Sciences of the United*
658 *States of America* **98**, 2053-2058.
659 **Moschopoulos, A., Derbyshire, P. and Byrne, M. E.** (2012). The Arabidopsis organelle-localized
660 glycyl-tRNA synthetase encoded by EMBRYO DEFECTIVE DEVELOPMENT1 is required for
661 organ patterning. *Journal of experimental botany* **63**, 5233-5243.
662 **Moulin, M., McCormac, A. C., Terry, M. J. and Smith, A. G.** (2008). Tetrapyrrole profiling in
663 Arabidopsis seedlings reveals that retrograde plastid nuclear signaling is not due to Mg-
664 protoporphyrin IX accumulation. *Proceedings of the National Academy of Sciences of the*
665 *United States of America* **105**, 15178-15183.
666 **Myouga, F., Hosoda, C., Umezawa, T., Iizumi, H., Kuromori, T., Motohashi, R., Shono, Y., Nagata,**
667 **N., Ikeuchi, M. and Shinozaki, K.** (2008). A heterocomplex of iron superoxide dismutases
668 defends chloroplast nucleoids against oxidative stress and is essential for chloroplast
669 development in Arabidopsis. *The Plant cell* **20**, 3148-3162.
670 **Neff, M. M., Neff, J. D., Chory, J. and Pepper, A. E.** (1998). dCAPS, a simple technique for the
671 genetic analysis of single nucleotide polymorphisms: experimental applications in Arabidopsis
672 thaliana genetics. *The Plant journal : for cell and molecular biology* **14**, 387-392.
673 **Neuhaus, H. E. and Emes, M. J.** (2000). Nonphotosynthetic Metabolism in Plastids. *Annu Rev Plant*
674 *Physiol Plant Mol Biol* **51**, 111-140.
675 **Nishiyama, R., Watanabe, Y., Fujita, Y., Le, D. T., Kojima, M., Werner, T., Vankova, R.,**
676 **Yamaguchi-Shinozaki, K., Shinozaki, K., Kakimoto, T., et al.** (2011). Analysis of cytokinin
677 mutants and regulation of cytokinin metabolic genes reveals important regulatory roles of
678 cytokinins in drought, salt and abscisic acid responses, and abscisic acid biosynthesis. *The*
679 *Plant cell* **23**, 2169-2183.

680 **Pelagio-Flores, R., Ortiz-Castro, R. and Lopez-Bucio, J.** (2013). dhm1, an Arabidopsis mutant with
681 increased sensitivity to alkamides shows tumorous shoot development and enhanced lateral
682 root formation. *Plant molecular biology* **81**, 609-625.
683 **Pogson, B. J., Woo, N. S., Forster, B. and Small, I. D.** (2008). Plastid signalling to the nucleus and
684 beyond. *Trends Plant Sci* **13**, 602-609.
685 **Pospisilova, J., Vagner, M., Malbeck, J., Travnickova, A. and Batkova, P.** Interactions between
686 abscisic acid and cytokinins during water stress and subsequent rehydration. *Biologia*
687 *Plantarum* **49**, 533-540.
688 **Prochazkova, D., Haisel, D. and Wilhelmova, N.** (2008). Antioxidant protection during ageing and
689 senescence in chloroplasts of tobacco with modulated life span. *Cell Biochem Funct* **26**, 582-
690 590.
691 **Ramel, F., Birtic, S., Ginies, C., Soubigou-Taconnat, L., Triantaphylides, C. and Havaux, M.**
692 (2012). Carotenoid oxidation products are stress signals that mediate gene responses to
693 singlet oxygen in plants. *Proceedings of the National Academy of Sciences of the United*
694 *States of America* **109**, 5535-5540.
695 **Schaller, G. E., Bishopp, A. and Kieber, J. J.** (2015). The yin-yang of hormones: cytokinin and auxin
696 interactions in plant development. *The Plant cell* **27**, 44-63.
697 **Schoof, H., Lenhard, M., Haecker, A., Mayer, K. F., Jurgens, G. and Laux, T.** (2000). The stem cell
698 population of Arabidopsis shoot meristems in maintained by a regulatory loop between the
699 CLAVATA and WUSCHEL genes. *Cell* **100**, 635-644.
700 **Schuster, C., Gaillochet, C., Medzihradszky, A., Busch, W., Daum, G., Krebs, M., Kehle, A. and**
701 **Lohmann, J. U.** (2014). A regulatory framework for shoot stem cell control integrating
702 metabolic, transcriptional, and phytohormone signals. *Developmental cell* **28**, 438-449.
703 **Scofield, S., Dewitte, W., Nieuwland, J. and Murray, J. A.** (2013). The Arabidopsis homeobox gene
704 SHOOT MERISTEMLESS has cellular and meristem-organisational roles with differential
705 requirements for cytokinin and CYCD3 activity. *The Plant journal : for cell and molecular*
706 *biology* **75**, 53-66.
707 **Sharma, S. and Verslues, P. E.** (2010). Mechanisms independent of abscisic acid (ABA) or proline
708 feedback have a predominant role in transcriptional regulation of proline metabolism during low
709 water potential and stress recovery. *Plant, cell & environment* **33**, 1838-1851.
710 **Skirycz, A., Claeys, H., De Bodt, S., Oikawa, A., Shinoda, S., Andriankaja, M., Maleux, K., Eloy,**
711 **N. B., Coppens, F., Yoo, S. D., et al.** (2011). Pause-and-stop: the effects of osmotic stress on
712 cell proliferation during early leaf development in Arabidopsis and a role for ethylene signaling
713 in cell cycle arrest. *The Plant cell* **23**, 1876-1888.

714 **Skoog, F. and Miller, C. O.** (1957). Chemical regulation of growth and organ formation in plant
715 tissues cultured in vitro. *Symp Soc Exp Biol* **11**, 118-130.
716 **Sun, X., Feng, P., Xu, X., Guo, H., Ma, J., Chi, W., Lin, R., Lu, C. and Zhang, L.** (2011). A
717 chloroplast envelope-bound PHD transcription factor mediates chloroplast signals to the
718 nucleus. *Nat Commun* **2**, 477.
719 **Sunkar, R., Kapoor, A. and Zhu, J. K.** (2006). Posttranscriptional induction of two Cu/Zn superoxide
720 dismutase genes in Arabidopsis is mediated by downregulation of miR398 and important for
721 oxidative stress tolerance. *The Plant cell* **18**, 2051-2065.
722 **Szabados, L. and Savoure, A.** (2010). Proline: a multifunctional amino acid. *Trends Plant Sci* **15**, 89-
723 97.
724 **Szekely, G., Abraham, E., Cseplo, A., Rigo, G., Zsigmond, L., Csiszar, J., Ayaydin, F., Strizhov,**
725 **N., Jasik, J., Schmelzer, E., et al.** (2008). Duplicated P5CS genes of Arabidopsis play distinct
726 roles in stress regulation and developmental control of proline biosynthesis. *The Plant journal :*
727 *for cell and molecular biology* **53**, 11-28.
728 **Tameshige, T., Fujita, H., Watanabe, K., Toyokura, K., Kondo, M., Tatematsu, K., Matsumoto, N.,**
729 **Tsugeki, R., Kawaguchi, M., Nishimura, M., et al.** (2013). Pattern dynamics in adaxial-
730 abaxial specific gene expression are modulated by a plastid retrograde signal during
731 Arabidopsis thaliana leaf development. *PLoS Genet* **9**, e1003655.
732 **To, J. P., Deruere, J., Maxwell, B. B., Morris, V. F., Hutchison, C. E., Ferreira, F. J., Schaller, G. E.**
733 **and Kieber, J. J.** (2007). Cytokinin regulates type-A Arabidopsis Response Regulator activity
734 and protein stability via two-component phosphorelay. *The Plant cell* **19**, 3901-3914.
735 **Ueguchi, C., Koizumi, H., Suzuki, T. and Mizuno, T.** (2001). Novel family of sensor histidine kinase
736 genes in Arabidopsis thaliana. *Plant & cell physiology* **42**, 231-235.
737 **Uhlken, C., Horvath, B., Stadler, R., Sauer, N. and Weingartner, M.** (2014). MAIN-LIKE1 is a
738 crucial factor for correct cell division and differentiation in Arabidopsis thaliana. *The Plant*
739 *journal : for cell and molecular biology* **78**, 107-120.
740 **Veley, K. M., Marshburn, S., Clure, C. E. and Haswell, E. S.** (2012). Mechanosensitive channels
741 protect plastids from hypoosmotic stress during normal plant growth. *Current biology : CB* **22**,
742 408-413.
743 **Verslues, P. E. and Sharma, S.** (2010). Proline metabolism and its implications for plant-environment
744 interaction. *The Arabidopsis book / American Society of Plant Biologists* **8**, e0140.
745 **Wagner, D., Przybyla, D., Op den Camp, R., Kim, C., Landgraf, F., Lee, K. P., Wursch, M., Laloi,**
746 **C., Nater, M., Hideg, E., et al.** (2004). The genetic basis of singlet oxygen-induced stress
747 responses of Arabidopsis thaliana. *Science* **306**, 1183-1185.

748 **Wilson, M. E., Basu, M. R., Bhaskara, G. B., Verslues, P. E. and Haswell, E. S.** (2014). Plastid
749 osmotic stress activates cellular stress responses in Arabidopsis. *Plant physiology* **165**, 119-
750 128.
751 **Wilson, M. E., Jensen, G. S. and Haswell, E. S.** (2011). Two mechanosensitive channel homologs
752 influence division ring placement in Arabidopsis chloroplasts. *The Plant cell* **23**, 2939-2949.
753 **Woodson, J. D. and Chory, J.** (2012). Organelle signaling: how stressed chloroplasts communicate
754 with the nucleus. *Current biology : CB* **22**, R690-692.
755 **Woodson, J. D., Perez-Ruiz, J. M. and Chory, J.** (2011). Heme synthesis by plastid ferrochelatase I
756 regulates nuclear gene expression in plants. *Current biology : CB* **21**, 897-903.
757 **Wu, A., Allu, A. D., Garapati, P., Siddiqui, H., Dortay, H., Zanor, M. I., Asensi-Fabado, M. A.,**
758 **Munne-Bosch, S., Antonio, C., Tohge, T., et al.** (2012). JUNGBRUNNEN1, a reactive
759 oxygen species-responsive NAC transcription factor, regulates longevity in Arabidopsis. *The*
760 *Plant cell* **24**, 482-506.
761 **Wysocka-Diller, J. W., Helariutta, Y., Fukaki, H., Malamy, J. E. and Benfey, P. N.** (2000).
762 Molecular analysis of SCARECROW function reveals a radial patterning mechanism common
763 to root and shoot. *Development* **127**, 595-603.
764 **Xiao, Y., Savchenko, T., Baidoo, E. E., Chehab, W. E., Hayden, D. M., Tolstikov, V., Corwin, J. A.,**
765 **Kliebenstein, D. J., Keasling, J. D. and Dehesh, K.** (2012). Retrograde signaling by the
766 plastidial metabolite MEcPP regulates expression of nuclear stress-response genes. *Cell* **149**,
767 1525-1535.
768 **Yamada, H., Suzuki, T., Terada, K., Takei, K., Ishikawa, K., Miwa, K., Yamashino, T. and Mizuno,**
769 **T.** (2001). The Arabidopsis AHK4 histidine kinase is a cytokinin-binding receptor that
770 transduces cytokinin signals across the membrane. *Plant & cell physiology* **42**, 1017-1023.
771 **Zhang, Z. W., Feng, L. Y., Cheng, J., Tang, H., Xu, F., Zhu, F., Zhao, Z. Y., Yuan, M., Chen, Y. E.,**
772 **Wang, J. H., et al.** (2013). The roles of two transcription factors, ABI4 and CBFA, in ABA and
773 plastid signalling and stress responses. *Plant molecular biology* **83**, 445-458.
774 **Zhao, Z., Andersen, S. U., Ljung, K., Dolezal, K., Miotk, A., Schultheiss, S. J. and Lohmann, J. U.**
775 (2010). Hormonal control of the shoot stem-cell niche. *Nature* **465**, 1089-1092.
776 **Zurcher, E., Tavor-Deslex, D., Lituiev, D., Enkerli, K., Tarr, P. T. and Muller, B.** (2013). A robust
777 and sensitive synthetic sensor to monitor the transcriptional output of the cytokinin signaling
778 network in planta. *Plant physiology* **161**, 1066-1075.
779
780
781 **FIGURE LEGENDS**

782

783 **Fig. 1. *msl2 msl3* double mutants develop callus at the shoot apex.** (A-D) Bright-field images
784 representative of phenotypes observed in 21-day-old *msl2 msl3* seedlings grown on solid media.
785 Shooty callus is indicated with a white arrowhead in (D). (E) Representative images of callus formation
786 over time. (F) Average percent of *msl2 msl3* seedlings with visible callus at the indicated time after
787 germination. 5 plates of seedlings, n > 10 seedlings per plate, were analyzed per time point. (G) The
788 average percent of *msl2 msl3* seedlings showing visible callus at 21 DAG after transfer from MS to MS
789 (black bars) or to MS supplemented with 82 mM NaCl (grey bars) at the indicated time points. 3 plates
790 of seedlings, n > 10 seedlings per plate, were analyzed per treatment. (F and G) Error bars = SEM. *,
791 difference from mock treatment, $P < 0.01$ (Student's *t*-test). (H) Representative bright-field images of
792 the aerial portion of 21-day-old seedlings scored in (G) (top row) or seedlings transferred from MS
793 supplemented with 82 mM NaCl to MS at indicated time points (bottom row). Size bars (A-E), 1 mm,
794 (H), 5 mm.

795

796 **Fig. 2. MSL2 function is required in the PZ/CZ/SAM to prevent callus production.** Transmission
797 electron microscope (TEM) images of *msl2 msl3* mutant SAM (A) and developing chloroplasts (B-C)
798 and proplastids (D-F) in 4-day-old wild type and *msl2 msl3* mutant seedlings. Examples of proplastids
799 and developing chloroplasts are indicated in *msl2 msl3* mutant by asterisks and black arrowheads,
800 respectively. Size bar = 10 μm (A-C), 1 μm (D), and 100 nm (E-F). Plastoglobules (PG), double
801 membrane (white arrowheads), and thylakoids (double black arrowheads) are indicated. (E) Magnified
802 region of *msl2 msl3* plastid envelope, indicated by box in D. (F) Representative bright-field images of
803 14-day-old *msl2 msl3* seedlings expressing the genomic version of MSL2 (*MSL2g*) or *MSL2* under the
804 control of the *SCR* promoter. Size bar = 5 mm.

805

806 **Fig. 3. Callus produced in *msl2 msl3* mutants is the result of increased CK production or**
807 **signaling.** (A) Representative bright-field images of seedlings grown for 21 days on solid media
808 containing the indicated concentration of the synthetic auxin NAA. Size bar = 1 mm. (B) Confocal
809 micrographs of non-green plastids in the first true leaf of *msl2 msl3* mutants harboring the RecA-
810 dsRED plastid marker and grown on MS media or media containing 82 mM NaCl or 2 μM NAA. Size
811 bar = 10 μm. (C) Percent of *msl2 msl3* mutants exhibiting callus when grown on NAA. The average of
812 three biological replicates of ≥ 20 seedlings each is presented. (D) trans-Zeatin-riboside and IAA
813 levels 21-day-old seedlings determined by LC MS/MS analysis. The average of three biological
814 replicates of ≥ 30 seedlings each is presented. Error bars indicate SD, *, $P < 0.01$ (Student's *t*-test).
815 Representative bright-field images (E) and callus production (F) of *msl2 msl3 ahk2-2* triple mutant

816 seedlings and parental lines. Size bar = 1 mm. The average of four biological replicates of ≥ 20
817 seedlings each is presented. Error bars indicate SEM, *$P < 0.01$ (Student's *t*-test). (G) Quantitative
818 RT-PCR analysis of *WUS*, *STM*, and A-type *ARR* gene expression. The average of three biological
819 replicates (two technical replicates; n ≥ 25 seedlings each) is presented. Error bars indicate SEM.
820
821 **Fig. 4. Preventing Pro biosynthesis results in a dramatic increase in callus formation in the**
822 ***msl2 msl3* background. (**A) Production of apical callus in *msl2 msl3* and *msl2 msl3 p5cs1-4*
823 seedlings in the presence and absence of exogenously provided Pro. The average of three biological
824 replicates is presented, $n \geq 25$ seedlings each. Error bars represent SD. (B) Pro content of the aerial
825 tissue of mutant and wild-type seedlings grown as in (A). The average of two biological replicates
826 (each performed in triplicate; n ≥ 30 seedlings each) is presented. (A) and (B) *, difference from *msl2*
827 *msl3*, $P < 0.01$ (Student's *t*-test). (C) Images of the meristematic region of representative seedlings
828 stained with DAB or NBT. Size bar = 1 mm. Quantification of H_2O_2 content by Amplex Red (D) and O_2^-
829 production by NBT-Formazan production (E) in mutant and wild-type seedlings of indicated age. The
830 average of three biological replicates ($n \geq 20$ seedlings each), two technical replicates each, is
831 presented in both (D) and (E). Error bars indicate SEM**. *,** difference from the wild type, $P < 0.01$
832 (Student's *t*-test). FW, fresh weight.
833
834 **Fig. 5. Hyperaccumulation of superoxide is required for callus formation in *msl2 msl3* and**
835 ***msl2 msl3 p5cs1* seedlings.** (A) NBT stained seedlings provided with TEMPOL or NaCl at 0, 3 or 7
836 DAG. Size bar = 1mm. (B) Callus production in double and triple mutant seedlings when grown on MS,
837 MS supplemented with 1 mM TEMPOL or MS supplemented with 82 mM NaCl. (C) Confocal
838 micrographs of non-green plastids in the first true leaf of *msl2 msl3* mutants harboring the RecA-
839 dsRED plastid marker grown on the indicated media. Size bar = 10 μm. (D) Apical callus production in
840 T2 lines segregating transgenes that over-express *CSD2* or *mCSD2*. The average of 4 biological
841 replicates ($n \geq 35$ seedlings each replicate) is presented. Error bars indicate SD. *, difference from
842 *msl2 msl3*, $P < 0.01$ (Student's *t*-test). (E) Percent of seedlings from (D) stained with NBT
843 accumulating formazan at the shoot apex. ($n \geq 20$ seedlings). (F) Representative bright-field images of
844 *CSD2* over-expression T2 lines. Size bar = 1 mm.
845
846 **Fig. 6. Callus production requires ABA biosynthesis, GUN1 and ABI4.** (A) Representative bright-
847 field images of 21-day-old *msl2 msl3 aba2-1* seedlings with relevant parental controls. (B) Callus
848 production in higher order mutants at 21 DAG. The average of 3 biological replicates ($n \geq 15$ seedlings
849 per replicate) is presented. Error bars indicate SEM. (C) Representative bright-field images of 21-day-

850 old *msl2 msl3 gun1-9* (+/-) and *msl2 msl3 gun1-9* (-/-) siblings at 21 DAG. (D) *msl2 msl3 abi4-1*
851 Representative bright-field images of 21-day-old *msl2 msl3 abi4-1* seedlings with relevant parental
852 controls. (E) Representative images of 21-day-old seedlings of the indicated genotypes stained with
853 DAB or NBT. Size bar = 1 mm.
854
855 **Fig. 7. Working Model.** These results are consistent with a working model wherein plastid osmotic
856 stress impacts both a feedback loop regulating cell proliferation in the shoot apical meristem (SAM)
857 (based on (Gaillochet et al., 2015) and a plastid ROS-dependent retrograde signaling pathway (Leon
858 et al., 2012). Plastid dysfunction leads to increased proliferation at the SAM and the production of
859 callus through increased CK levels and *WUS* expression and through an unknown nuclear
860 transcription program triggered by GUN1, ABA, and ABI4.

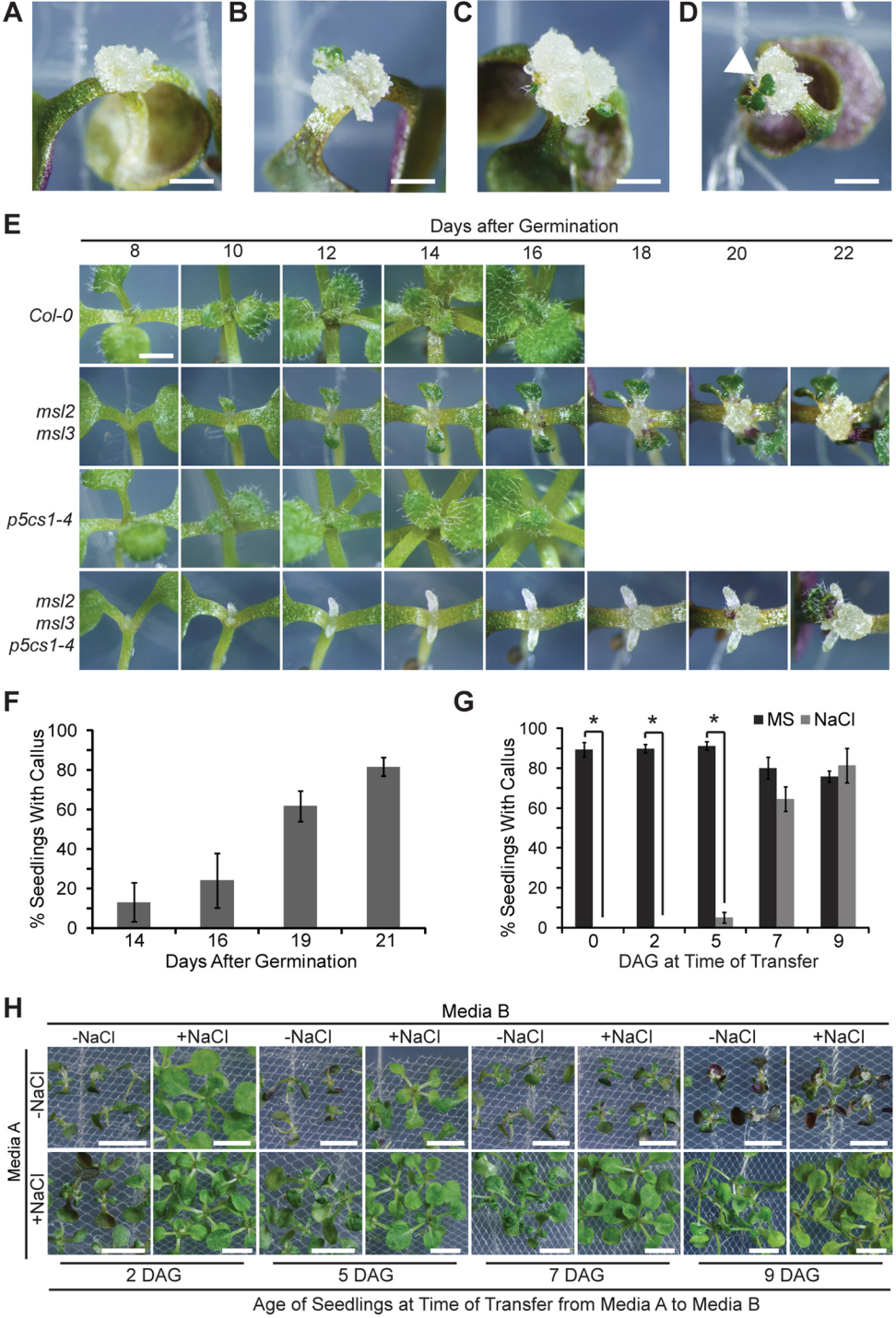

Fig. 1. *msl2 msl3* double mutants develop callus at the shoot apex. (A-D) Bright-field images representative of phenotypes observed in 21-day-old *msl2 msl3* seedlings grown on solid media. Shooty callus is indicated with a white arrowhead in (D). (E) Representative images of callus formation over time. (F) Average percent of *msl2 msl3* seedlings with visible callus at the indicated time after germination. 5 plates of seedlings, n > 10 seedlings per plate, were analyzed per time point. (G) The average percent of *msl2 msl3* seedlings showing visible callus at 21 DAG after transfer from MS to MS (black bars) or to MS supplemented with 82 mM NaCl (grey bars) at the indicated time points. 3 plates of seedlings, n > 10 seedlings per plate, were analyzed per treatment. (F and G) Error bars = SEM. *, difference from mock treatment, $P < 0.01$ (Student's *t*-test). (H) Representative bright-field images of the aerial portion of 21-day-old seedlings scored in (G) (top row) or seedlings transferred from MS supplemented with 82 mM NaCl to MS at indicated time points (bottom row). Size bars (A-E), 1 mm, (H), 5 mm.

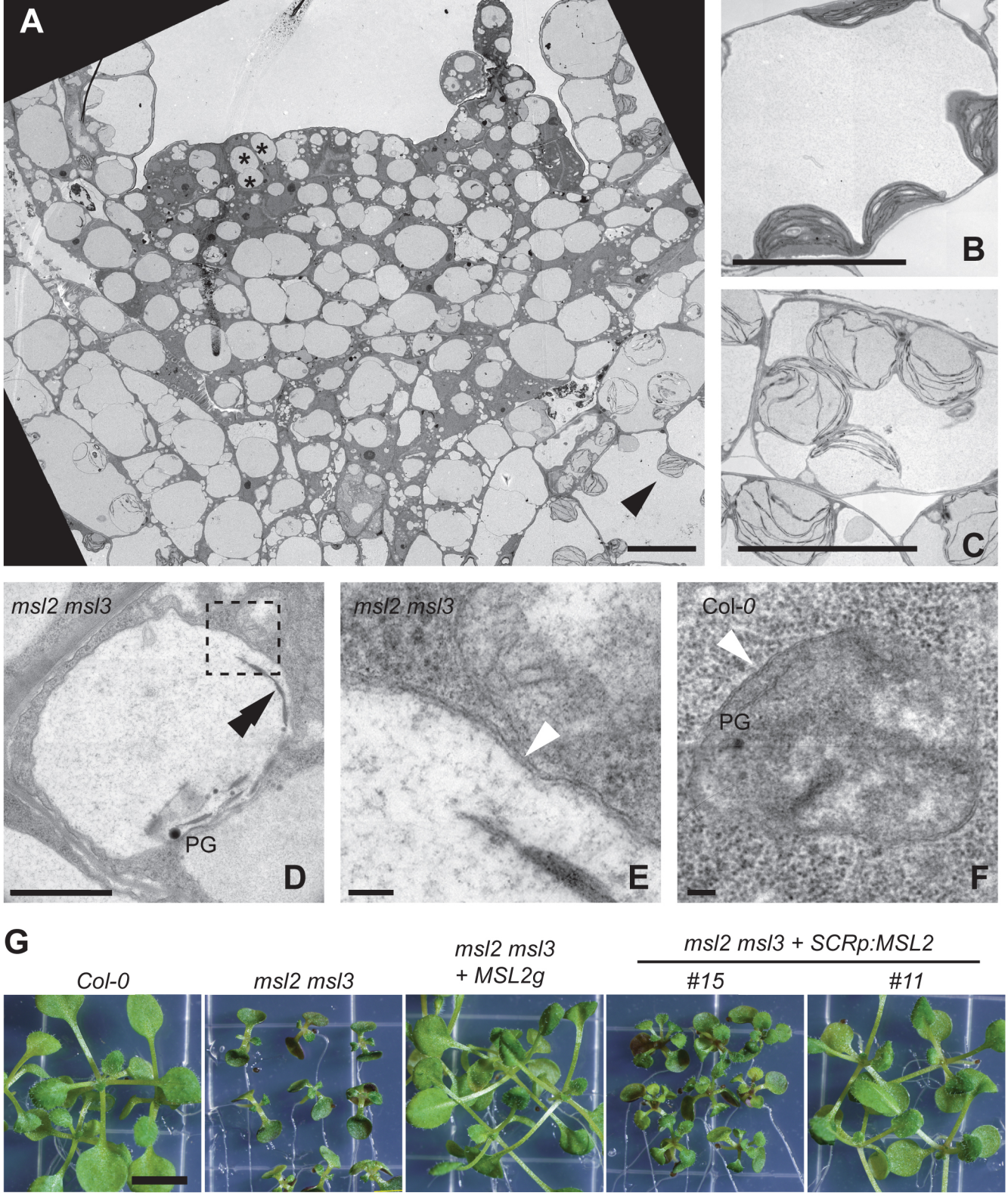

Fig. 2. MSL2 function is required in the PZ/CZ/SAM to prevent callus production. Transmission electron microscope (TEM) images of *msl2 msl3* mutant SAM (A) and developing chloroplasts (B-C) and proplastids (D-F) in 4-day-old wild type and *msl2 msl3* mutant seedlings. Examples of proplastids and developing chloroplasts are indicated in *msl2 msl3* mutant by asterisks and black arrowheads, respectively. Size bar = 10 μm (A-C), 1 μm (D), and 100 nm (E-F). Plastoglobules (PG), double membrane (white arrowheads), and thylakoids (double black arrowheads) are indicated. (E) Magnified region of *msl2 msl3* plastid envelope, indicated by box in D. (F) Representative bright-field images of 14-day-old *msl2 msl3* seedlings expressing the genomic version of MSL2 (*MSL2g*) or *MSL2* under the control of the *SCR* promoter. Size bar = 5 mm.

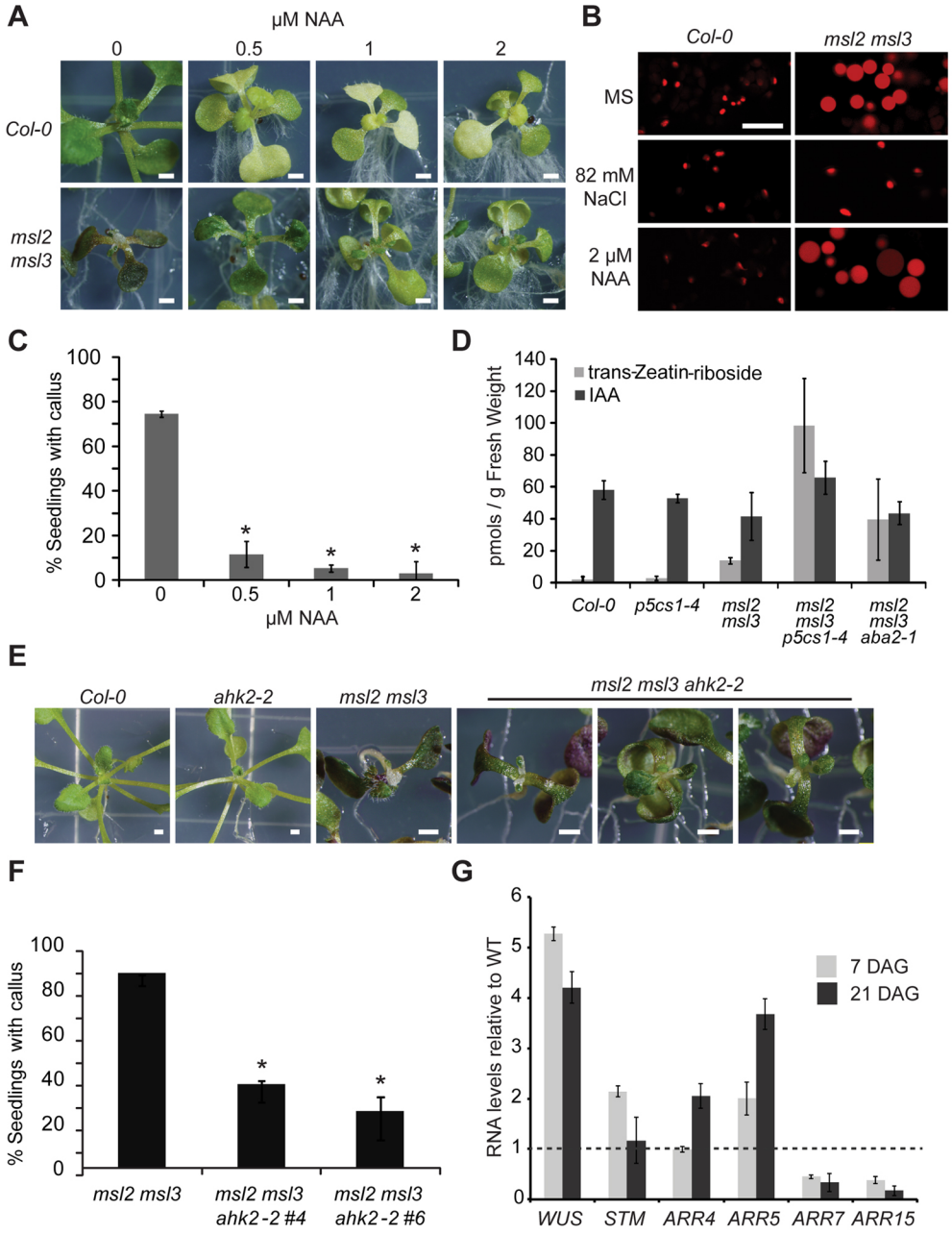

Fig. 3. Callus produced in *msl2 msl3* mutants is the result of increased CK production or signaling. (A) Representative bright-field images of seedlings grown for 21 days on solid media containing the indicated concentration of the synthetic auxin NAA. Size bar = 1 mm. (B) Confocal micrographs of non-green plastids in the first true leaf of *msl2 msl3* mutants harboring the RecA-dsRED plastid marker and grown on MS media or media containing 82 mM NaCl or 2 μM NAA. Size bar = 10 μm. (C) Percent of *msl2 msl3* mutants exhibiting callus when grown on NAA. The average of three biological replicates of ≥ 20 seedlings each is presented. (D) trans-Zeatin-riboside and IAA levels 21-day-old seedlings determined by LC MS/MS analysis. The average of three biological replicates of ≥ 30 seedlings each is presented. Error bars indicate SD, *, $P < 0.01$ (Student's *t*-test). Representative bright-field images (E) and callus production (F) of *msl2 msl3 ahk2-2* triple mutant seedlings and parental lines. Size bar = 1 mm. The average of four biological replicates of ≥ 20 seedlings each is presented. Error bars indicate SEM, *$P < 0.01$ (Student's *t*-test). (G) Quantitative RT-PCR analysis of *WUS*, *STM*, and A-type *ARR* gene expression. The average of three biological replicates (two technical replicates; n ≥ 25 seedlings each) is presented. Error bars indicate SEM.

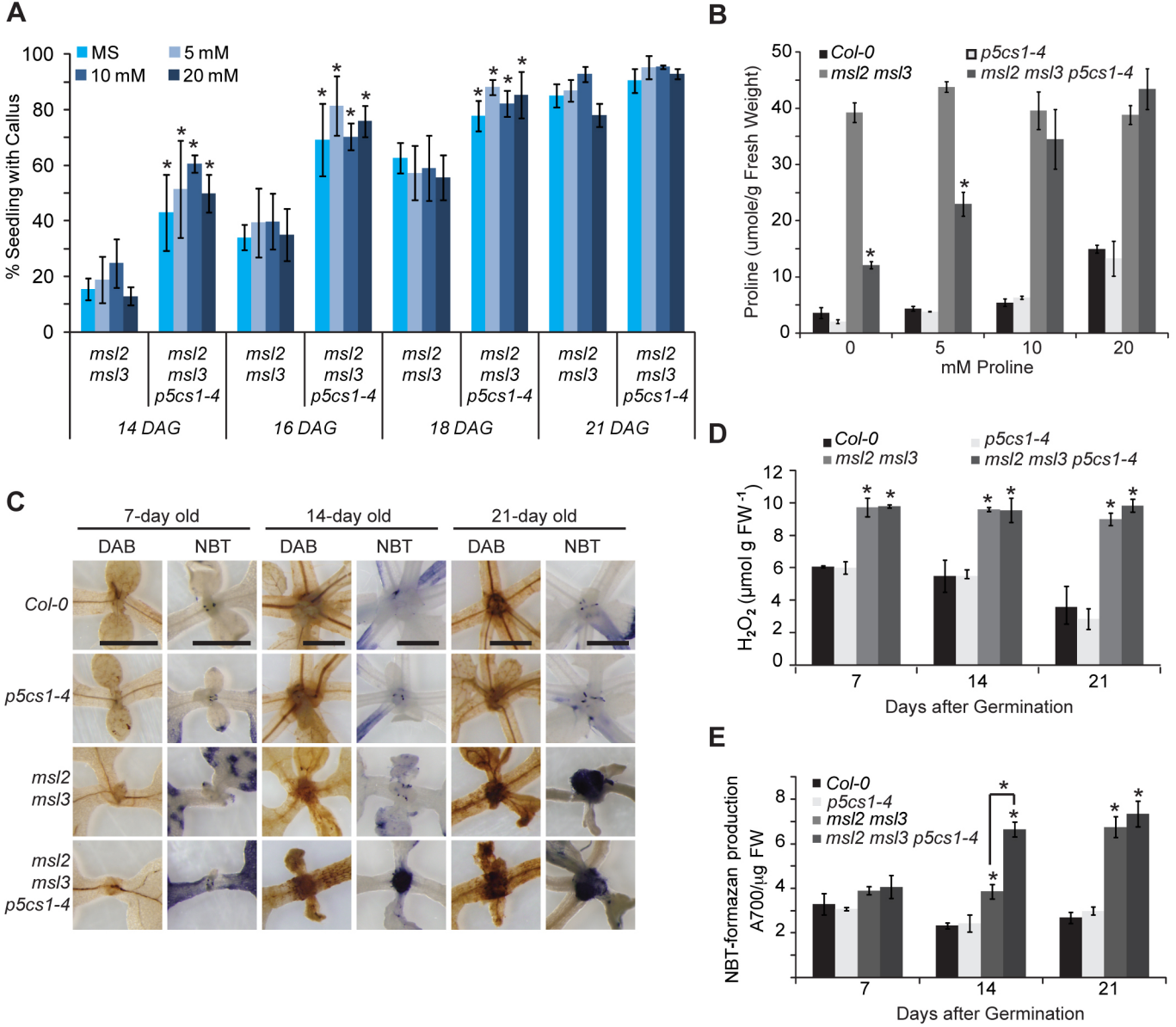

Fig. 4. Preventing Pro biosynthesis results in a dramatic increase in callus formation in the *msl2 msl3* background. (A) Production of apical callus in *msl2 msl3* and *msl2 msl3 p5cs1-4* seedlings in the presence and absence of exogenously provided Pro. The average of three biological replicates is presented, $n \geq 25$ seedlings each. Error bars represent SD. (B) Pro content of the aerial tissue of mutant and wild-type seedlings grown as in (A). The average of two biological replicates (each performed in triplicate; n ≥ 30 seedlings each) is presented. (A) and (B) *, difference from *msl2 msl3*, $P < 0.01$ (Student's *t*-test). (C) Images of the meristematic region of representative seedlings stained with DAB or NBT. Size bar = 1 mm. Quantification of H_2O_2 content by Amplex Red (D) and O_2^- production by NBT-Formazan production (E) in mutant and wild-type seedlings of indicated age. The average of three biological replicates ($n \geq 20$ seedlings each), two technical replicates each, is presented in both (D) and (E). Error bars indicate SEM. *, difference from the wild type, $P < 0.01$ (Student's *t*-test). FW, fresh weight.

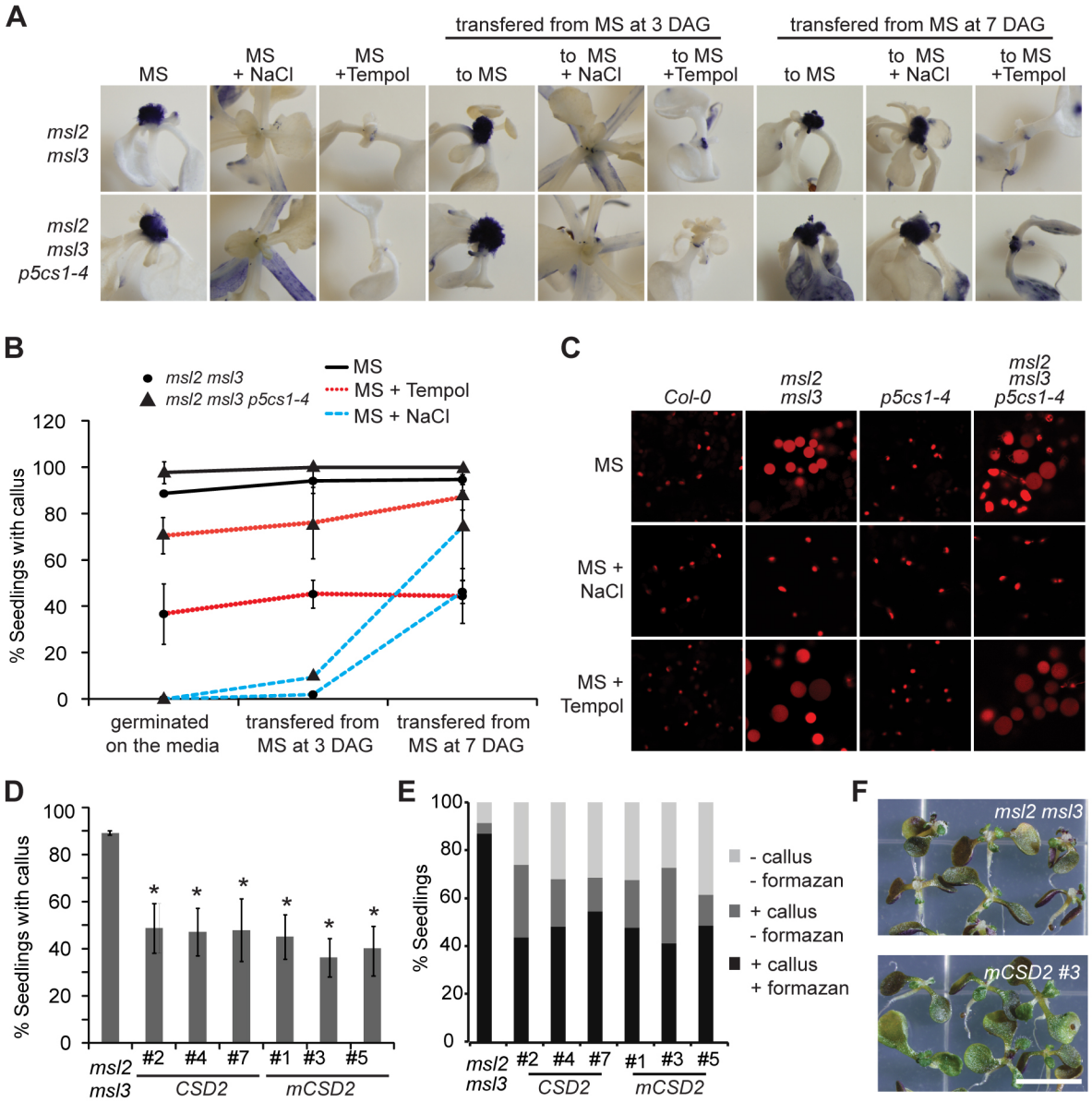

Fig. 5. Hyperaccumulation of superoxide is required for callus formation in *msl2 msl3* and *msl2 msl3 p5cs1* seedlings. (A) NBT stained seedlings provided with TEMPOL or NaCl at 0, 3 or 7 DAG. Size bar = 1mm. (B) Callus production in double and triple mutant seedlings when grown on MS, MS supplemented with 1 mM TEMPOL or MS supplemented with 82 mM NaCl. (C) Confocal micrographs of non-green plastids in the first true leaf of *msl2 msl3* mutants harboring the RecA-dsRED plastid marker grown on the indicated media. Size bar = 10 μm. (D) Apical callus production in T2 lines segregating transgenes that over-express *CSD2* or *mCSD2*. The average of 4 biological replicates ($n \geq 35$ seedlings each replicate) is presented. Error bars indicate SD. *, difference from *msl2 msl3*, $P < 0.01$ (Student's *t*-test). (E) Percent of seedlings from (D) stained with NBT accumulating formazan at the shoot apex. ($n \geq 20$ seedlings). (F) Representative bright-field images of *CSD2* over-expression T2 lines. Size bar = 1 mm.

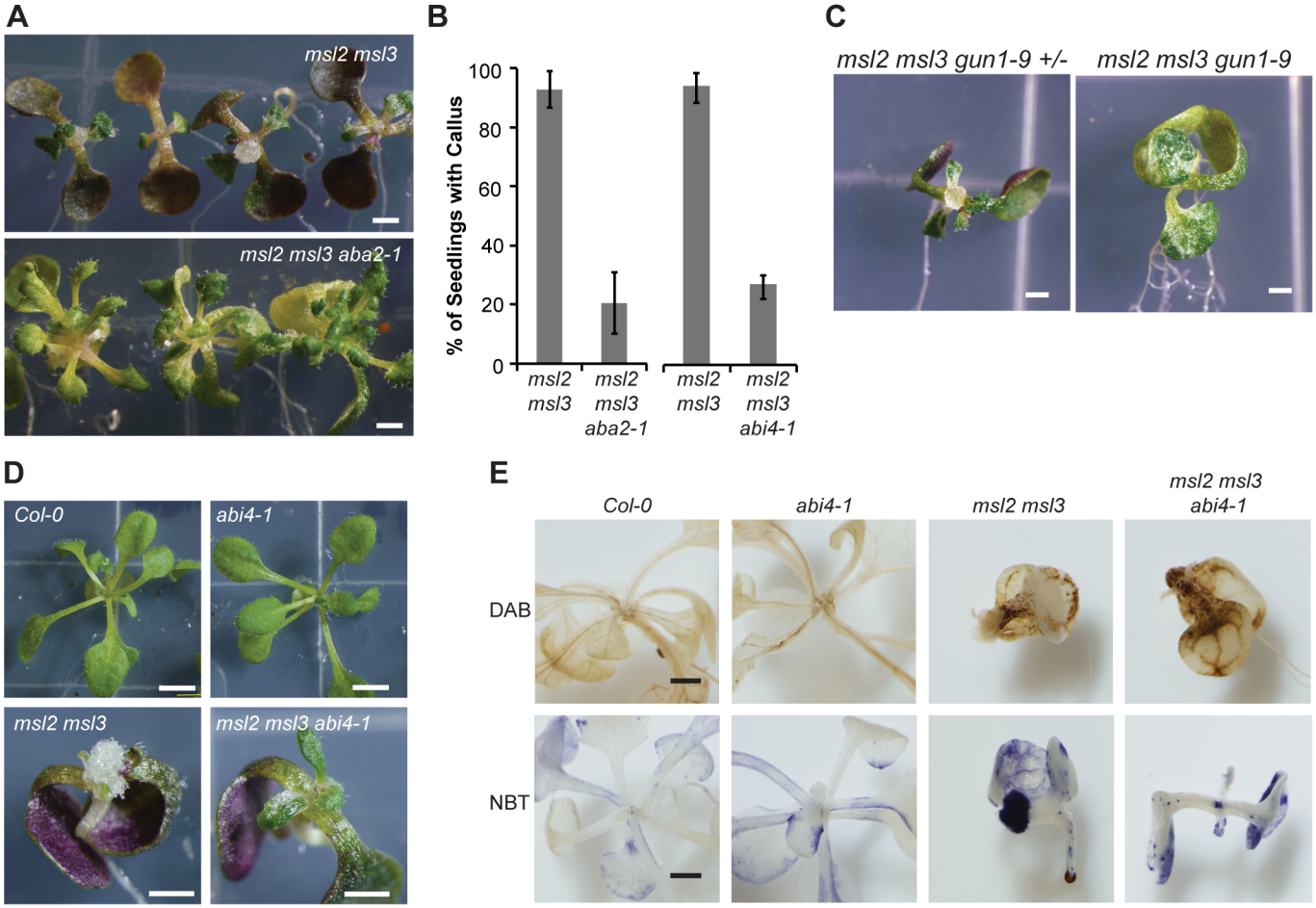

Fig. 6. Callus production requires ABA biosynthesis, GUN1 and ABI4. (A) Representative bright-field images of 21-day-old *msl2 msl3 aba2-1* seedlings with relevant parental controls. (B) Callus production in higher order mutants at 21 DAG. The average of 3 biological replicates ($n \geq 15$ seedlings per replicate) is presented. Error bars indicate SEM. (C) Representative bright-field images of 21-day-old *msl2 msl3 gun1-9* (+/-) and *msl2 msl3 gun1-9* (-/-) siblings at 21 DAG. (D) *msl2 msl3 abi4-1* Representative bright-field images of 21-day-old *msl2 msl3 abi4-1* seedlings with relevant parental controls. (E) Representative images of 21-day-old seedlings of the indicated genotypes stained with DAB or NBT. Size bar = 1 mm.

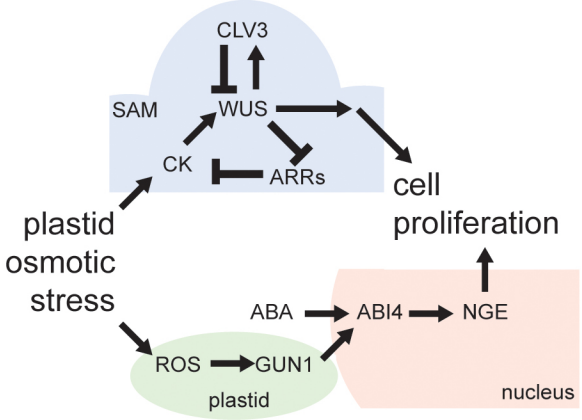

Fig. 7. Working Model. These results are consistent with a working model wherein plastid osmotic stress impacts both a feedback loop regulating cell proliferation in the shoot apical meristem (SAM) (based on (Gaillochet et al., 2015) and a plastid ROS-dependent retrograde signaling pathway (Leon et al., 2012). Plastid dysfunction leads to increased proliferation at the SAM and the production of callus through increased CK levels and *WUS* expression and through an unknown nuclear transcription program triggered by GUN1, ABA, and ABI4.